UNCLASSIFIED DTIC FILE COPY

(2)

AD-A199 930

DTIC ELECTE JUL 26 1988 S D

DOCUMENTATION PAGE

Form Approved OMB No. 0704-0188

1b. RESTRICTIVE MARKINGS	
2a. SECURITY CLASSIFICATION AUTHORITY	3. DISTRIBUTION/AVAILABILITY OF REPORT: Approved for Public Release; Distribution is unlimited.
2b. DECLASSIFICATION/DOWNGRADING SCHEDULE	
4. PERFORMING ORGANIZATION REPORT NUMBER(S): Mechanics and Engineering Science	5. MONITORING ORGANIZATION REPORT NUMBER(S): AFOSR-TR- 88-0956
6a. NAME OF PERFORMING ORGANIZATION: Dept. of Aero. Engr., Mechs., and Eng. Science	6b. OFFICE SYMBOL (If applicable):
6c. ADDRESS (City, State, and ZIP Code): University of Florida, Gainesville, Florida 32611	7a. NAME OF MONITORING ORGANIZATION: AFOSR/NA
	7b. ADDRESS (City, State, and ZIP Code): BollingAir Force Base, Washington, DC 20332-6448 BN41C
8a. NAME OF FUNDING/SPONSORING ORGANIZATION: Air Force Office of Scientific Research	8b. OFFICE SYMBOL (If applicable): AFOSR/NA
8c. ADDRESS (City, State, and ZIP Code): Bolling Air Force Base, D.C. 20332 BN41C	9. PROCUREMENT INSTRUMENT IDENTIFICATION NUMBER: AFOSR-87-0201
	10. SOURCE OF FUNDING NUMBERS: PROGRAM ELEMENT NO. 61102F; PROJECT NO. 2302; TASK NO. C2; WORK UNIT ACCESSION NO.

11. TITLE (Include Security Classification): Strength and Deformation of Confined and Unconfined Concrete Under Axial Dynamic Loading (UNCLASSIFIED)

12. PERSONAL AUTHOR(S): Malvern Lawrence E., and Jenkins, David A.

13a. TYPE OF REPORT	13b. TIME COVERED	14. DATE OF REPORT (Year, Month, Day)	15. PAGE COUNT
Final Technical	FROM 870515 TO 880714	1988 August 24	71

16. SUPPLEMENTARY NOTATION

17. COSATI CODES			18. SUBJECT TERMS (Continue on reverse if necessary and identify by block number)
FIELD	GROUP	SUB-GROUP	Concrete, Dynamic Loads, Dynamic Properties, Dynamic Testing, Fracture, Hopkinson Bar, ~~Impact (continued)~~

19. ABSTRACT (Continue on reverse if necessary and identify by block number)

This report describes a research program whose specific objectives were to develop procedures and to demonstrate the feasibility of using them to make micrographic examinations of slices cut from damaged Split-Hopkinson-Pressure Bar unconfined concrete compression test specimens that were recovered intact and also from untested and statically tested specimens in order to determine crack development characteristics. The general objective was to obtain a qualitative understanding of the physical mechanism leading to failure and potentially a quantitative basis for deformation and failure process modeling. This specific investigation was preliminary for a more extensive study of both confined and unconfined test specimens.

(continued on reverse side)

20. DISTRIBUTION/AVAILABILITY OF ABSTRACT	21. ABSTRACT SECURITY CLASSIFICATION	
☒ UNCLASSIFIED/UNLIMITED ☐ SAME AS RPT ☐ DTIC USERS	UNCLASSIFIED	
22a. NAME OF RESPONSIBLE INDIVIDUAL: Dr. Spencer Wu	22b. TELEPHONE (Include Area Code): (202) 767-6962	22c. OFFICE SYMBOL: AFOSR/NA

DD Form 1473, JUN 86 — Previous editions are obsolete. — SECURITY CLASSIFICATION OF THIS PAGE

UNCLASSIFIED

Block 18 (continued) Kolsky Bar Apparatus, Materials Testing, Rate Effects, Petrographic Examination.

Block 19 (continued)

A method of interrupting the test by means of a loosely fitting steel collar permitted intact specimens to be recovered from both regimes before and after the peak stress. Procedures of furfural alcohol infiltration and polymerization were developed, which successfully stabilized the crack patterns before grinding and polishing the slices for micrographic examination. From the limited amount of data obtained it appears that a substantial increase in crack density occurs at a threshold strain near the peak stress. The crack density was considerably higher in dynamic tests than in static tests at the same level of maximum strain. Further investigation is needed to explore the regime leading up to the threshold, involving closer examination to observe microcracks not seen in this study.

STRENGTH AND DEFORMATION OF CONFINED AND UNCONFINED CONCRETE UNDER AXIAL DYNAMIC LOADING

FINAL REPORT

LAWRENCE E. MALVERN

DAVID A. JENKINS

DEPARTMENT OF AEROSPACE ENGINEERING, MECHANICS,

AND ENGINEERING SCIENCE

UNIVERSITY OF FLORIDA

GAINESVILLE, FLORIDA 32611

24 AUGUST 1988

U.S. AIR FORCE OFFICE OF SCIENTIFIC RESEARCH

CONTRACT NUMBER AFOSR-87-0201

UNIVERSITY OF FLORIDA

PREFACE

This is the final technical report on a research program sponsored by the U. S. Air Force Office of Scientific Research, Directorate of Aerospace Sciences, Bldg. 410, Bolling Air Force Base, D. C., 20332. Program Manager for the Air Force is Dr. Spencer Wu. This final report describes the technical effort during the period from 15 May 1987 through 14 July 1988.

The contractor is the University of Florida, Division of Sponsored Research, 219 Grinter Hall, Gainesville, Florida 32611. The research was performed by personnel of the Department of Aerospace Engineering, Mechanics, and Engineering Sciences, University of Florida, Gainesville, Florida, 32611, at the Gainesville campus of the University. Co-Principal Investigators are Professor Lawrence E. Malvern and Dr. David A. Jenkins.

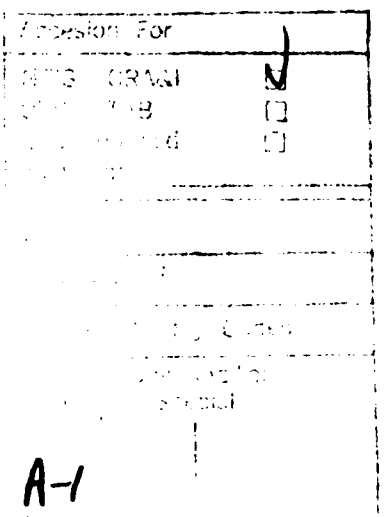

TABLE OF CONTENTS

LIST OF FIGURES

LIST OF APPENDIX FIGURES

LIST OF TABLES

SECTION I

INTRODUCTION

The objectives of the research reported here were to develop procedures and demonstrate the feasibility of using them to make micrographic examinations of undamaged and damaged Split-Hopkinson-Pressure-Bar (SHPB) compression specimens in order to determine crack development characteristics in the impacted specimens. Several previously proposed models for concrete failure under impact involve crack initiation, propagation and coalescence assumptions, which had so far not been verified by observations of the crack patterns after varying amounts of damage before general failure. The general objective then was to attempt to make such observations, whose results could provide a qualitative understanding of the physical mechanism leading to failure and potentially a quantitative basis for deformation and failure process modeling, when a sufficient data base has been accumulated.

In order to accomplish the objective two experimental procedures had first to be developed. The most difficult one was the petrographic procedure with which the specimen crack pattern in a longitudinal slice was stabilized by furfural alcohol infiltration and polymerization to fill the cracks with a rigid furan resin before the slice was mounted and polished for

micrographic examination. Without this procedure additional cracks would be introduced by the preparation of the micrographic examination slice. Some details of the preparation and micrographic examination procedures are summarized in Section 3.2.

The other problem that had to be overcome was recovering specimens with various amounts of deformation before complete failure. To this end a steel collar was placed around each specimen. The inside diameter of the collar was sufficiently large that it did not provide lateral confinement. Specimens were cut slightly longer than the collar, and then the ends were ground to assure flatness and parallelism and to produce a range of excess lengths of the order of from 0.0012 to 0.012 times the collar length. Thus after an axial strain of 0.0012 to 0.012 the steel collar began to stop the loading, and indeed the collar sufficiently inhibited further axial deformation that an intact specimen could be retrieved even when it was extensively cracked. Details of the testing procedure are given in Section 3.1. Similar collar tests were performed quasistatically at comparable levels of axial deformation, and the crack patterns are compared to the patterns from the dynamic tests.

Section II is a background section reviewing the SHPB testing facility and referring to previous reports where more comprehensive historical accounts may be found of various

approaches to obtaining a better understanding of the response of concrete and concrete structures to impulsive loadings, which is needed as a foundation on which to base both designs for adequate protective structures and plans for munitions that can defeat protective structures.

Section II is followed by Section III on experimental procedures of the present investigation, and then Section IV gives test results and discussion. Conclusions and recommendations for further research are presented in Section V.

SECTION II

DYNAMIC TESTING WITH THE SPLIT HOPKINSON PRESSURE BAR

A detailed literature survey on dynamic testing has been published in a 1986 paper, Reference 1, which also presented results obtained up to that time on high-strength concrete specimens in the split Hopkinson Pressure Bar (SHPB) system at the University of Florida under an AFOSR contract. Additional results were reported in the final report of that contract, Reference 2. Some earlier papers gave additional details of the system, preliminary results on high-strength concrete, Reference 3, and some results on mortar in a smaller system, Reference 4. Only a brief description of the SHPB system and its use will be given here.

A Kolsky Apparatus or Split Hopkinson's Pressure Bar (SHPB) system with 3-inch (76.2 mm) diameter pressure bars has been built at the University of Florida for dynamic compression of specimens up to 3 inches (76.2 mm) in diameter.

The SHPB system consists of two long strain-gaged pressure bars with a short specimen sandwiched between them. Analysis of the observed longitudinal elastic stress waves in the two pressure bars furnishes information about both the force and the displacement versus time at each of the two specimen interfaces. From this record the average stress and strain in the specimen is

deduced. Most of the existing SHPB systems in the world have a maximum specimen diameter of 1 inch (25.4 mm). In structures of interest, concrete aggregate sizes up to 0.5 inch (12.7 mm) or even larger may be used. For such concrete, a larger specimen must be used in order to obtain representative properties of the composite material. The new system was developed for this reason.

This facility is the only one of its kind in the United States. It has been used for unconfined dynamic testing of five different kinds of high-strength concrete prepared at Waterways Experiment Station, Terra-Tek Inc., and SRI International and also for testing SIFCON (slurry-infiltrated fiber concrete) furnished by the New Mexico Engineering Research Institute for AFWAL at strain rates from 5 to 200 per second.

As currently configured it provides a loading pulse lasting 300 microseconds, imparted by impact of the 30-inch (762 mm) striker bar against the incident pressure bar. The 120-inch-long (3.05-m-long) incident and transmitter pressure bars are mounted in pillow blocks supported by a steel frame structure. The whole system including gas gun, pressure bars and a shock absorber with 6.5-inch (165-mm) stroke at the far end is almost 30 feet (9.15 m) long. The projectile nose protrudes about 1.5 inches (38 mm) outside the muzzle of the gas gun when it strikes the incident pressure bar and may travel up to 8 inches (203 mm) farther

before the pressure bars are stopped by the crushing specimen and the shock absorber.

Figure 1 is a schematic of the pressure bar arrangement, with a Lagrange diagram above it illustrating the elastic wave propagation in the pressure bars. Figure 2 shows an example of the axial strain signals versus time, recorded by a Hewlett Packard 7470A digital plotter from the stored signals in the digital oscilloscope. Compressive strain is plotted upward. After the passage of the first incident pulse, of nominal length 300 microsec (from the beginning of the rise to the beginning of the fall), there is a dwell time before the arrival of the reflected pulse from the specimen, which is recorded at the same gage station as the incident pulse. Another channel shows the pulse transmitted through the concrete specimen into the transmitter bar. Because the two gage stations are approximately equidistant from the specimen, the transmitted pulse arrives at the transmitter-bar gage station at approximately the same time as the reflected pulse arrives back at the incident-bar station. The transmitted pulse in Figure 2 actually arrives about 16 microsec later than the reflected pulse. This delay is caused by the time of about 19 microsec required for the pulse to pass through the three-inch-long concrete specimen and close up any air gaps at the interfaces, decreased three microsec because the transmitter gage is slightly closer to the bar end than the incident gage is. Also shown are records from two strain gages

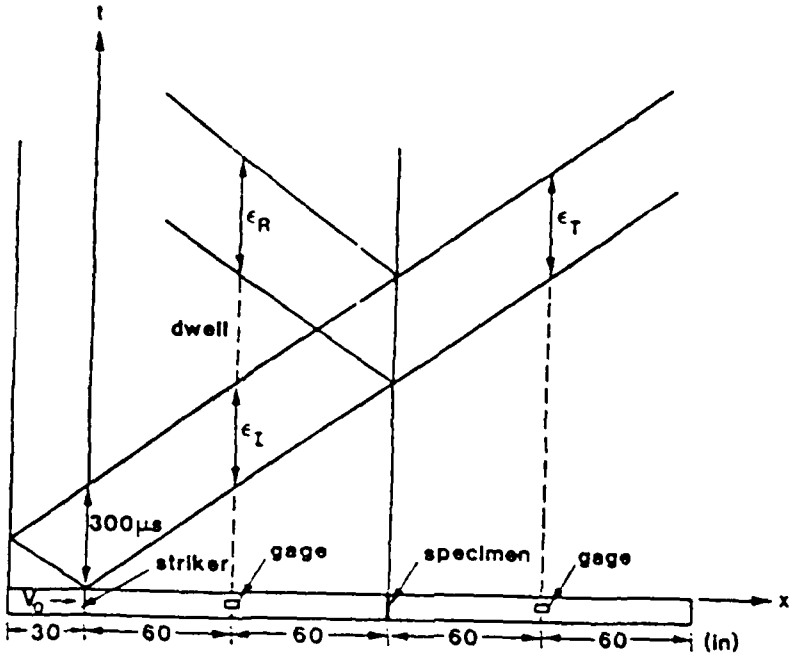

Figure 1. Schematic of SHPB Bars and Lagrange Diagram

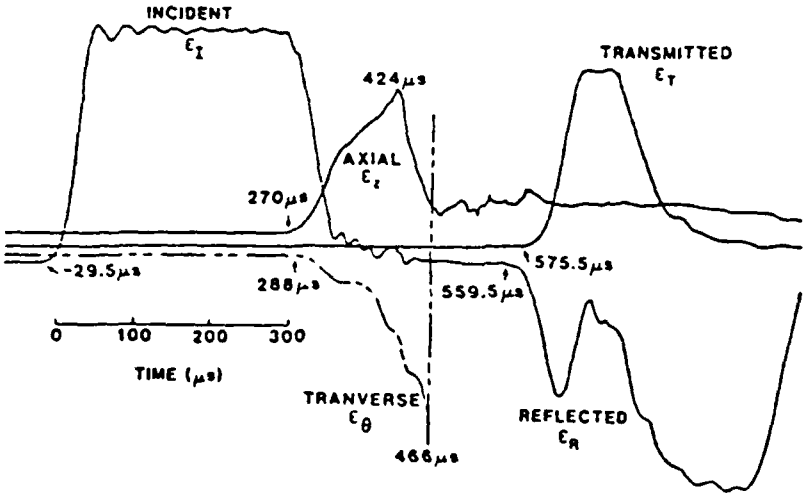

Figure 2. Strain Pulses in Pressure Bars and Axial and Transverse Specimen Surface Strains

mounted on the specimen midway between its ends, one measuring axial surface strain ϵ_z and one measuring transverse (hoop) strain ϵ_θ.

For purposes of analysis, as shown in Figures 3 to 6, the pulses are time shifted, so that time zero coincides with the arrival at the first specimen interface, and corrected for wave dispersion in the pressure bars, using a procedure developed under Task Order 85-6 from AFESC/RDC, Tyndall AFB, Florida. The dispersion-correction procedure is similar to that used by Follansbee and Frantz, Reference 5 and Felice, Reference 6, except that it uses a Fast Fourier Transform method instead of a Fourier series and therefore runs much faster on a computer.

Figure 3 shows both corrected and uncorrected time-shifted incident, reflected and transmitted pulses for the test of Figure 2. Although the corrected and uncorrected pulses appear to agree well, the differences in detail, especially for the incident and reflected pulses, which are added algebraically to obtain the pressure bar strain at the first specimen interface, lead to significant differences as may be seen in Figures 4 and 5. Figure 4 shows uncorrected first and second interface stresses, while Figure 5 shows corrected first and second interface stresses in the nominally three-inch-long (76.2 mm) specimen. The dispersion correction leads to much closer agreement of the two interface stresses, an approximate

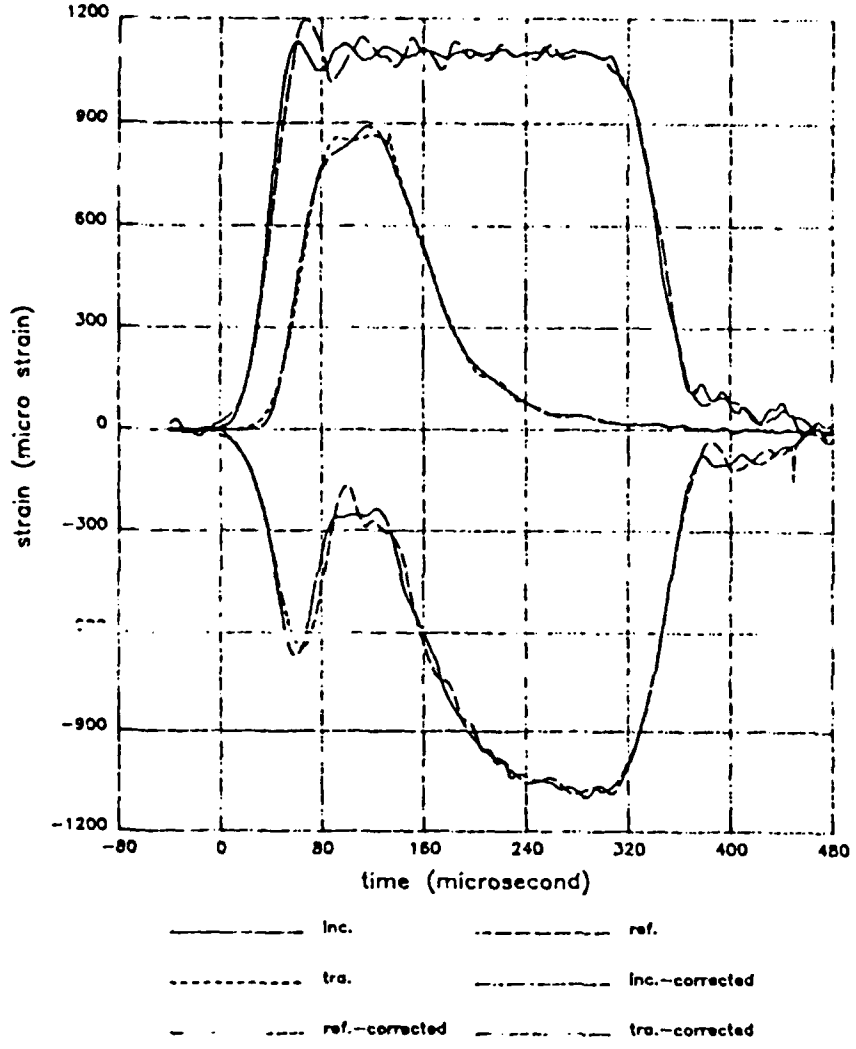

Figure 3. Incident, reflected and transmitted pulses (corrected and uncorrected) for the SHPB test.

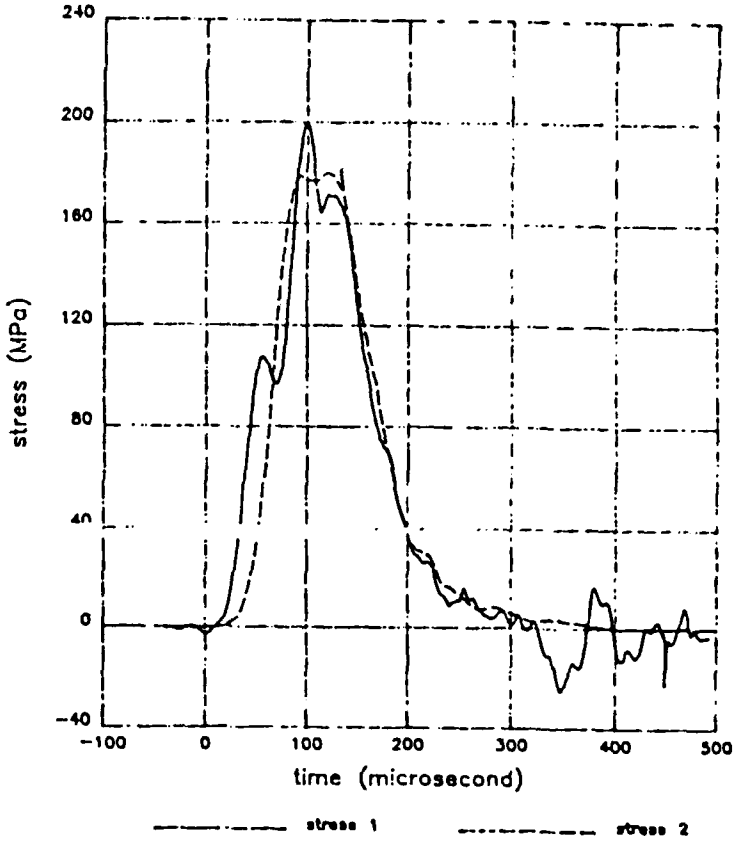

Figure 4. Uncorrected stresses at two specimer interfaces.

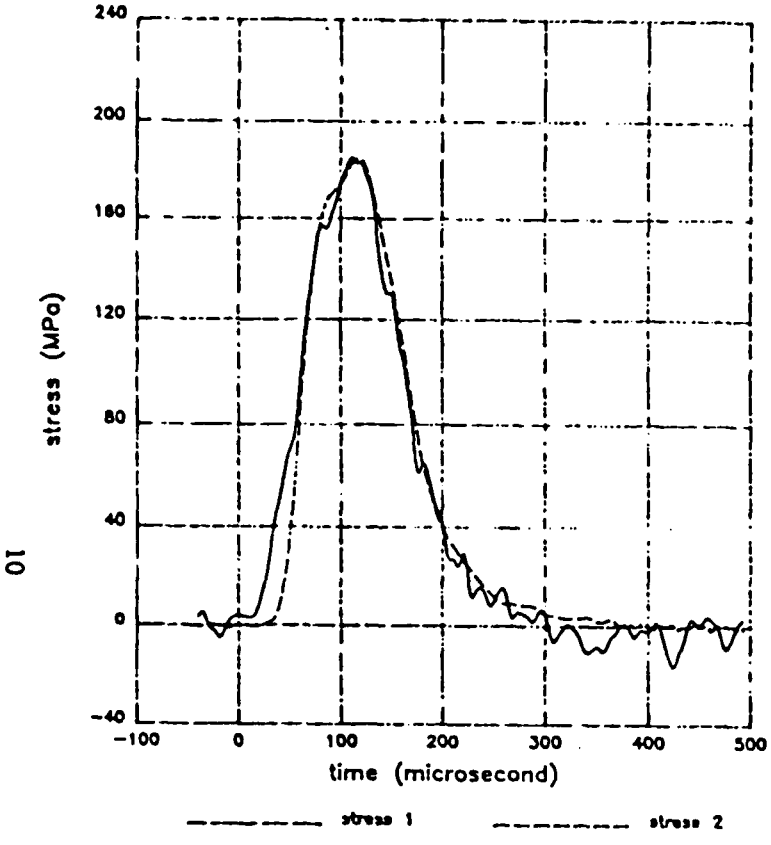

Figure 5. Corrected stresses at two specimen interfaces.

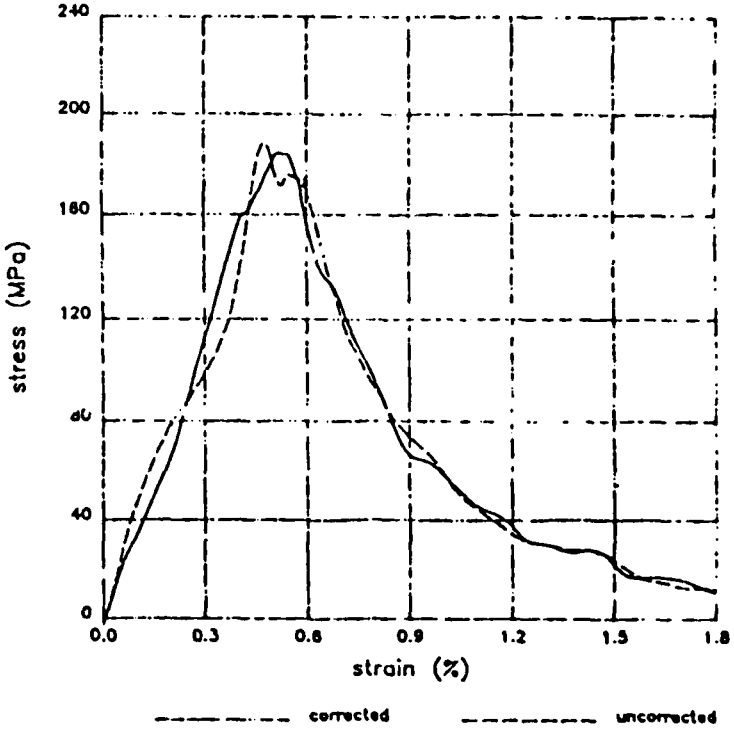

Figure 6. Corrected and uncorrected dynamic stress–strain curves.

equilibrium of the two stresses before they have reached half the maximum stress in this case. Figure 6 compares corrected and uncorrected stress-strain curves. The stress plotted is the arithmetic mean of the two interface stresses. The examples presented so far have all been for a high-strength concrete, prepared at the U.S. Army Waterways Experiment Station, which had a nominal unconfined static compressive strength on the order of 104 MPa (15 KSI) and unconfined dynamic strengths 50 to 100 per cent higher in SHPB tests than in the static tests, for strain rates at the maximum stress varying from 5 s^{-1} to 200 s^{-1}, as reported in Reference 1.

The results presented in the rest of this section and the following sections were obtained on a concrete of moderate strength prepared at the University of Florida. Unconfined static compressive strength was around 69 MPa (10KSI). Details of the mix are given in Section III. Strain pulses similar to those of Figure 2 were recorded in the pressure bars of the SHPB with an unconfined specimen of diameter 2 inches (50.8 mm) and nominal length 1.70 inches (43.2 mm). In this case no strain gages were mounted on the specimen.

In calculating specimen stresses account had to be taken of the differece in area between bars and specimen.

Specimen interface stresses and average strains and strain rates (averaged along specimen length) were computed, based on the analysis of the elastic waves in the pressure bars. Figure 7 shows the two interface stresses based on the elastic analysis without dispersion correction. Note the apparent large oscillation in the rising part of Stress 1. The cause of this is as follows. The first interface stress computation involves the algebraic addition of the incident and reflected pulses after appropriate time shifting to combine the pulses at the time when they were at the specimen interfaces. The two pulses being combined are of comparable over-all magnitudes, so that when the small oscillations on each of them are not properly phased, the combination leads to large oscillations in Stress 1. The oscillations on the recorded strain pulses are higher frequency components of the pulse, and their wave speed depends on frequency. Figure 8 shows the Stress 1 and Stress 2 curves for the same test, calculated with bar strain pulses corrected for elastic wave dispersion. The large oscillation in the rising part of Stress 1 has been removed by the correction procedure, and Stress 1 and Stress 2 pulses are similar, although the agreement is not as good as in Figure 5. Apparently the area mismatch between specimen and bars introduces additional oscillations in Stress 1.. The corrected Stress 2 is not greatly changed from the uncorrected Stress 2 of Figure 7, because its calculation did not involve a differencing procedure. Before the dispersion correction procedure was implemented, stress results

were usually based on Stress 2 because of the anomalous appearance of Stress 1.

It may still be a good idea to use only the corrected Stress 2 when the uncorrected Stress 1 has such large oscillations that the dispersion correction does not give a reasonable result. Figure 9 shows the two interface stresses and the specimen strain rate and strain all plotted versus time. The strain rate peaks at about 70 microseconds; it falls to a local minimum at about 95 microseconds, shortly after the stress maxima at around 88 to 91.5 microseconds, and then the strain rate increases again as the specimen stress is decreasing in the failure regime usually referred to as strain softening. In this case the first strain-rate peak is probably related to the approximately 70 microsecond rise time of the incident loading pulse. Note the three definitions of the ordinate scale. With strain, for example, a reading of 100 is to be multiplied by 1/10,000 to give 0.01 or 1 percent strain.

Figure 10 shows strain rate versus strain and two stress-strain curves. Stress 1 and Stress 2 are each plotted versus the average strain. The Stress 2 curve is believed to be the more reliable. According to it the maximum stress (general failure) occurs at a strain of 0.0064 for this test with a gas-gun firing pressure of 200 psi (1.378 MPa), which gave a striker-bar impact speed of 302 in/s (7.67 m/s).

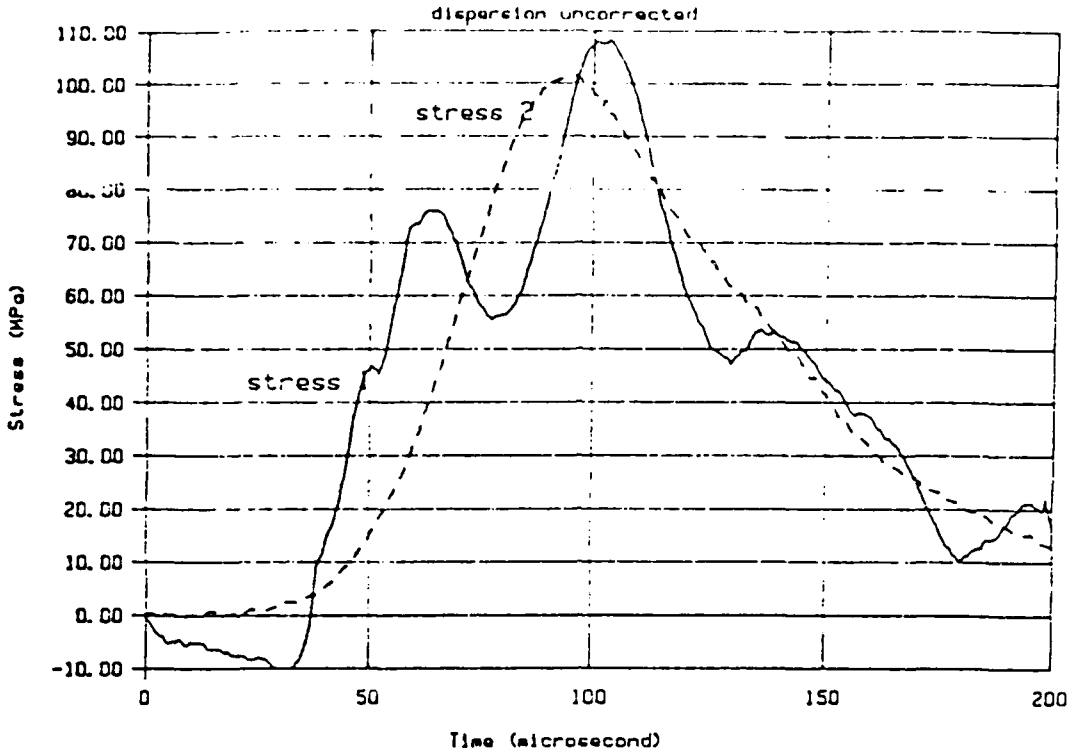

Figure 7. Uncorrected stresses at two interfaces for Specimen F05.

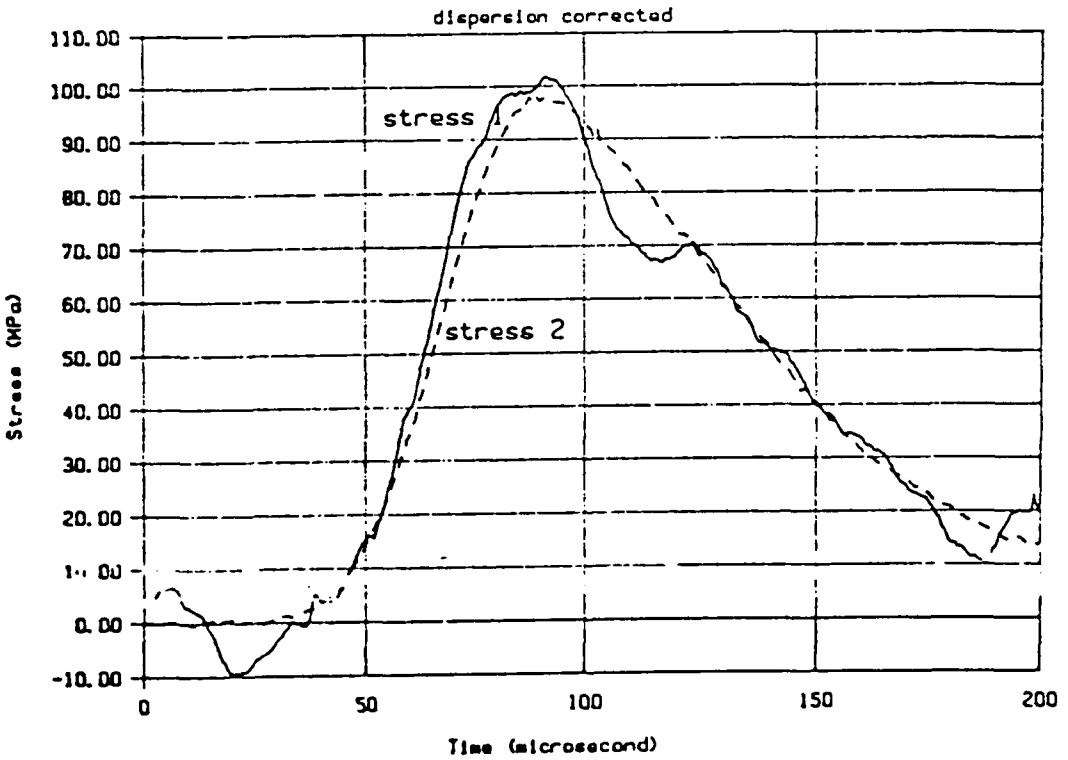

Figure 8. Dispersion-corrected stresses at two interfaces for Specimen F05.

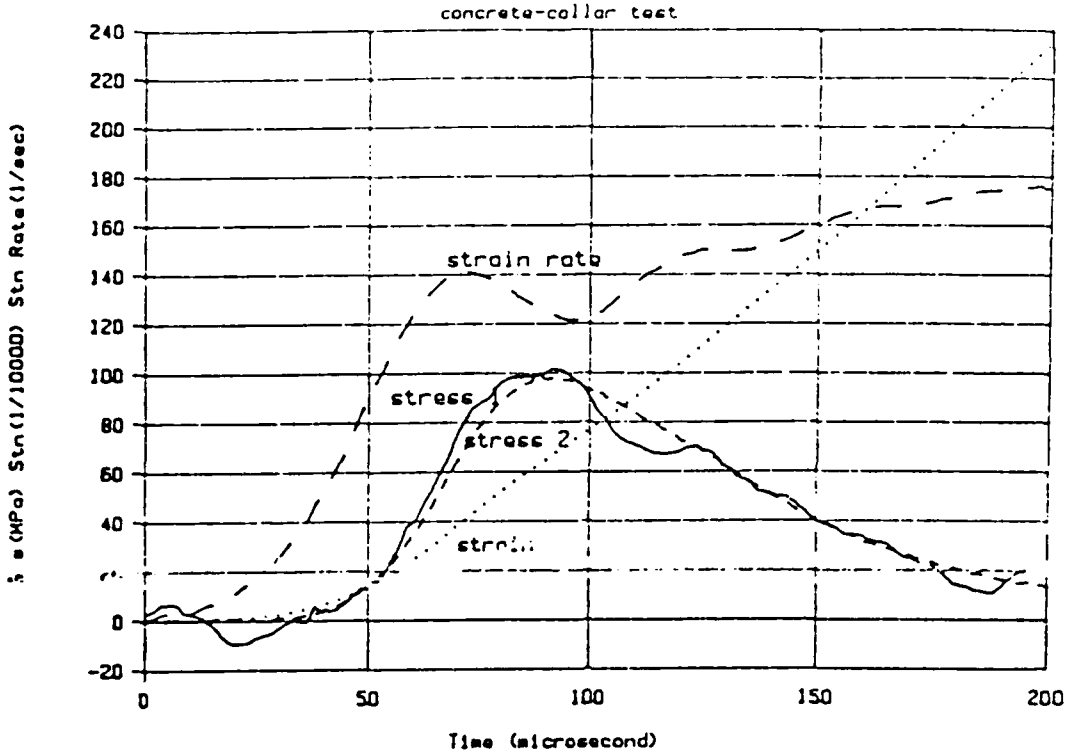

Figure 9. Stresses, strain, and strain rate versus time for Specimen F05.

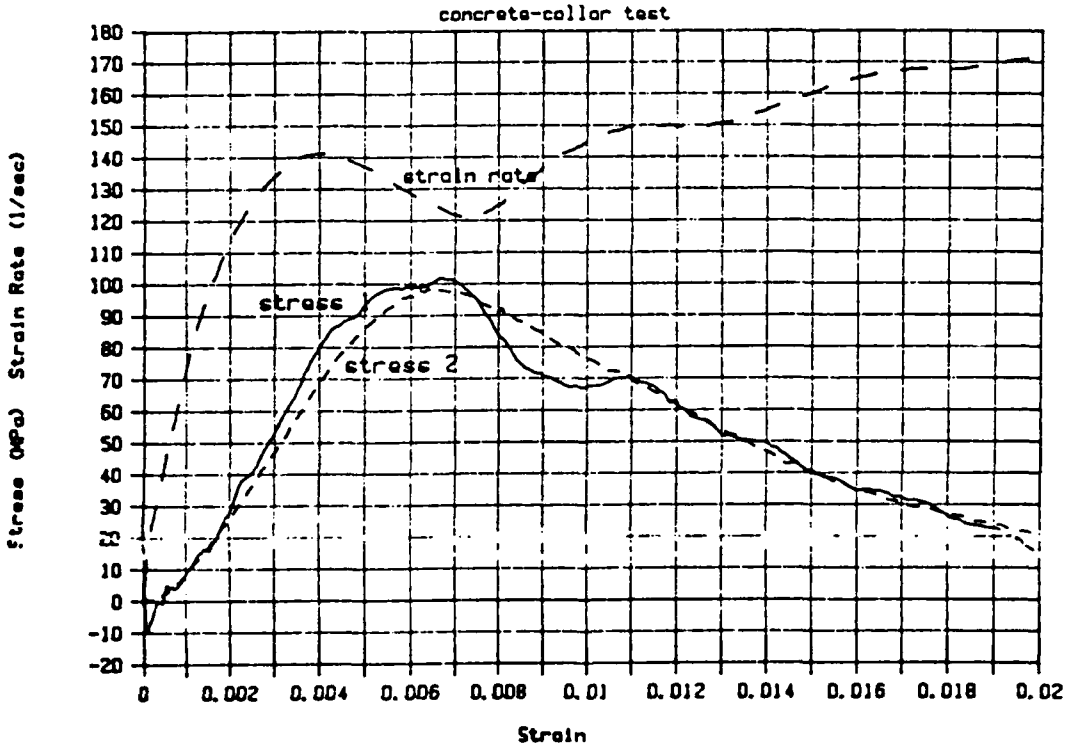

Figure 10. Stresses and strain rate versus strain for Specimen F05.

This same firing pressure was used in all the collar-interrupted tests to be described in Sections III and IV. Thus, if all the specimens had identical properties, when the specimen was enough longer than the collar that a strain of about 0.0064 or more was reached before the collar interrupted the test, the specimens recovered would be expected to be from the strain-softening regime.

SECTION III

EXPERIMENTAL PROCEDURES

3.1 Concrete Specimens and Test Procedures

Test material was cast in split tube molds with inside diameters of 2 inches (50.8 mm) and lengths of approximately 5 inches (127 mm). After curing, two test specimens 1.75 inches (44.5 mm) long were sawed from the central regions of the resulting cylinders. The ends of the specimens were then ground flat and parallel on a surface grinder using a special support fixture, to produce a series of finished lengths ranging from 1.709 to 1.727 inches (43.4 to 32.9 mm) for subsequent static and dynamic testing.

A steel collar 1.707 inches (43.36 mm) in length with a bore of 2.050 inches (52.1 mm) and an outside diameter of 3 inches (76.2 mm) was fabricated, with special care taken to insure that the ends were parallel and flat. This collar, which is shown in Figure 11 (not to scale) stopped each static and dynamic test near the desired level of total strain and helped maintain the integrity of the cracked specimens. The specimen lengths exceeded the collar length by amounts ranging from 0.0012 to 0.012 times the collar length. Thus after an axial strain in the concrete specimen of from 0.0012 to 0.012 the collar would begin to stop the loading.

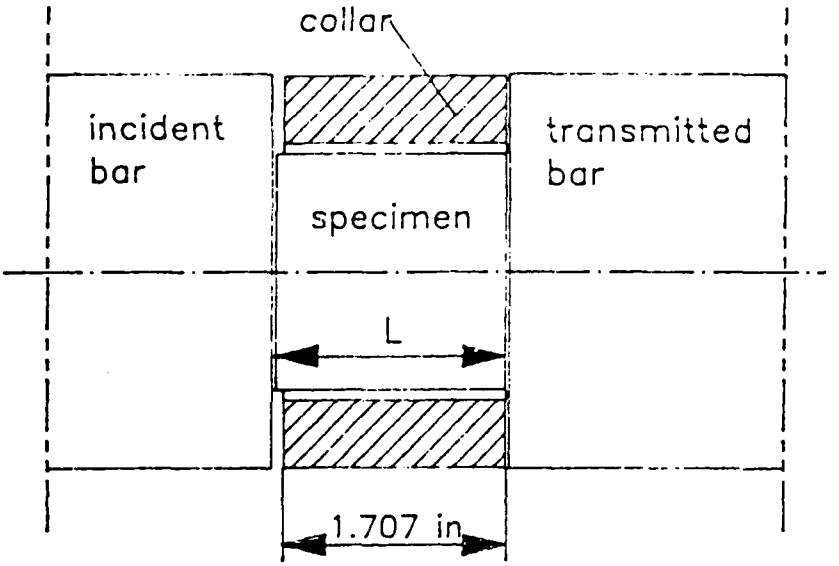

Figure 11. Sketch of collar used to interrupt tests.

The concrete mix used for this group of tests is shown in Table 1. The average density of the specimens was 2.22 g/cm^3.

Table 1. CONCRETE MIXTURE DESIGN

Type II Portland Cement	32.7 lb.
Brooksville Aggregate No. 89	94.2 lb.
Sand (Keuka, FL Pit No. 76-137)	60.4 lb.
Water	16.5 lb.
Water/Cement Ratio	0.50
Slump	2.25 inches

The Brooksville, Florida aggregate No. 89 is a mixture of coarse and fine manufactured Florida limestone aggregate with a maximum size of 3/8 inch (9.5 mm).

Two series of tests were conducted. One series, done in the SHPB described in Section II, will be referred to as the dynamic or high speed tests. The specimens in the high speed series were tested using a firing pressure of 200 psi (1.378 MPa) and were surrounded by the steel collar during the tests. As each specimen began to fail during the test, the steel collar came into contact with the incident and the transmitter bar, shifting the load from the specimen and effectively arresting the test near a pre-determined level of strain, hereafter referred to as the predicted strain. The six dynamic test specimens for which crack development was determined by the petrographic methods to be described in the following section were designed for predicted strains of 0.0029, 0.0047, 0.0064, 0.0081, 0.0099 and 0.0116 before the collar began to act. In each of the dynamic tests some further axial deformation of the specimen occurred along with the axial elastic shortening of the collar, so that the measured maximum strains (corresponding to the maximium crack development) were larger than the predicted strains by approximately 0.0002, as will be shown in Section IV.

The second series of tests was done using a hydraulic press to slowly apply the load and will be referred to as the static test series. Once again, the steel collar was used to arrest the test at a given level of strain and to prevent destroying the specimen. Petrographic examination was made of

six specimens with strain levels over a range comparable to that of the six dynamic tests, although the strains in the series are not exactly matched.

Section 3.2 describes petrographic preparation and examination procedures. In Section IV the results of the crack distribution observations in a longitudinal section of each specimen in the two test series will be presented and compared with each other and with a similar petrographic examination of an untested specimen.

3.2 Petrographic Examination Procedures

After each specimen was tested, it was stabilized by potting it in a polyester mounting resin (LECO Castolite), a procedure which helped keep the specimens together throughout subsequent handling. After curing of the polyester, a longitudinal slice approximately 0.060 inch (1.52 mm) thick was cut from the center of each specimen. Each slice was of course surrounded by a band of the polyester mounting resin, which continued to hold together the cracked material. The end of the slice which had been in contact with the incident bar was marked by making a small notch at the center.

In order to further stabilize the structure during mechanical polishing and to provide visual contrast to aid in

examination of the crack patterns, a procedure based on the infiltration and polymerization of furfural alcohol was used and is described here. The slices were first placed in a small vacuum chamber and immersed in a bath of approximately 50 cc of liquid furfural alcohol [2-$(C_4H_3O)CH_2OH$] . In order to eliminate trapped air and free water, a soft vacuum was pulled on the specimen and the bath using a mechanical vacuum pump. The vacuum was maintained for at least 20 minutes. Then atmospheric pressure was slowly introduced into the chamber, forcing the furfural alcohol deep into all cracks and crevices communicating with the surface. Approximately 20 drops of concentrated hydrochloric acid were then carefully added to the alcohol, initiating a polymerization reaction which causes the amber colored furfural alcohol to become a furan resin, which is rigid and dark brown in color. The contrasting color in the resin-filled cracks aided in their observation, and the rigidity of the system inhibited further crack development during polishing.

After removal from the furan resin mass, each slice was once again mounted in a polyester metallographic mount for ease of handling during mechanical polishing. The mounted specimens were ground flat by hand on a succession of silicon carbide grinding papers (180 - 320 - 600 grit), using no lubricant. Finally, each was polished using 6 micron diamond paste on a synthetic fiber polishing wheel, using kerosene as a lubricant.

A macrophotograph was made of each mounted section for later use in marking the paths of cracks. An example is shown in Figure 12. Macrophotographs of all 13 specimens examined are given in the appendix. Large cracks can be readily seen in the photographs, but smaller cracks can only be observed by using the metallographic microscope at 5 - 50X. A typical view through the microscope is shown in Figure 13. Because it was desired to generate an overall view of the emerging crack patterns, a routine was developed wherein the entire surface of the section was scanned using the microscope and any cracks that were found were marked on a large black and white print of the section

Figure 12. Typical macrophotograph of a tested, infiltrated and polished concrete specimen.

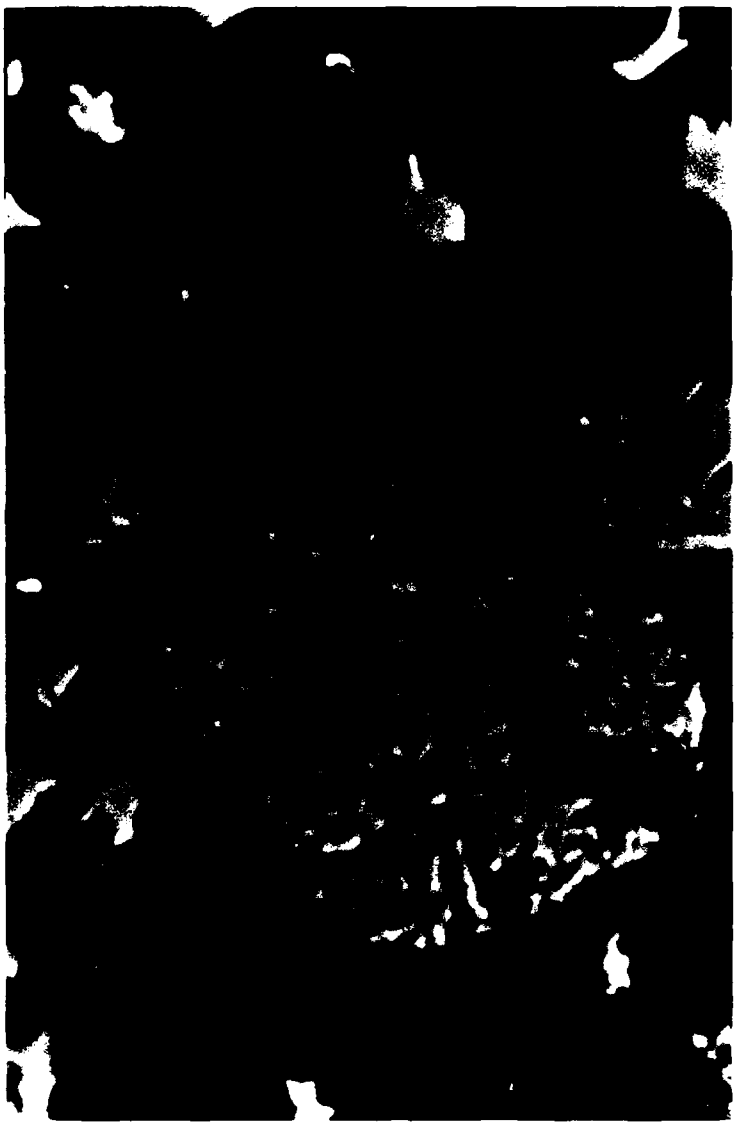

Figure 13. Typical micrograph taken at 50x showing furan-resin-filled cracks traversing mortar and an aggregate particle.

macrophotograph using a blue pen. This part of the effort was quite time consuming, but was considered to be unavoidable considering the difficulty in locating and identifying the cracks, a procedure that often involved some judgement on the part of the microscopist.

When the crack path marking was completed, tracings on plain white paper were made to isolate and enhance the crack patterns. In this form, the eye is not distracted by the other micrographic features present and the patterns are more easily analyzed.

To deduce the length of cracks per unit area in the cross section and the surface area of cracks per unit volume, the quantitative stereology technique of line intercept counting was employed. A grid of sample lines was laid over the traced crack pattern, as shown in the example of Figure 14, and the number of intercepts each sample line made with cracks was recorded. The total number of intercepts, divided by the total length of sample line, can be shown to be equal to $2/\pi$ times the crack length per unit area. The crack length per unit area can further be shown to equal $\pi/2$ times the total crack surface area per unit volume (counting both surfaces created by the crack), so that the intercept count per unit length gives the crack surface area per unit volume directly; see Underwood, Reference 7.

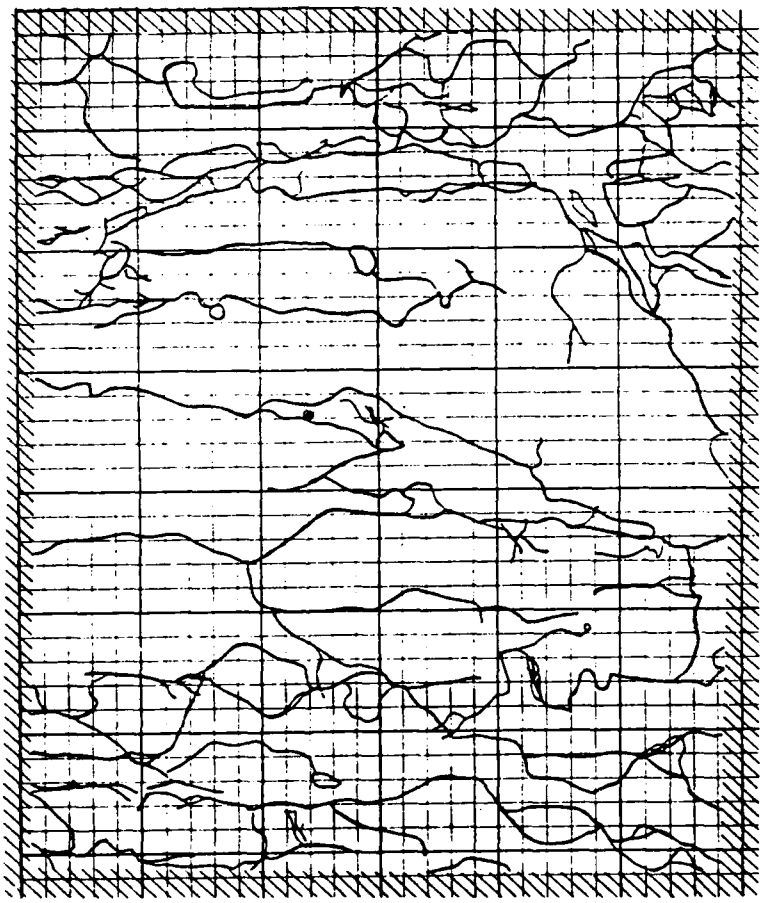

Figure 14. Example of crack pattern tracing overlaid with a grid of sample lines.

The line intercept method applies to internal surfaces of any shape and orientation provided random section planes and sample lines are used. Limited section orientations and sample line directions can cause systematic errors in the measurements if the internal surfaces have preferred orientations. The accuracy is also limited by the statistics of the sampling; observation of only one section through the specimen may entirely miss major features. In this case, a grid of approximately 40 X 40 sample lines extending completely across the specimen was used to obtain reasonable confidence for the measurement on the one section examined. Numerous sections would be required to get a true picture of the overall crack density throughout the specimen, but time constraints allowed only one section per test specimen.

SECTION IV

RESULTS

4.1 Observed Mechanical Behavior

The mechanical results of the dynamic tests terminated by the collar will be illustrated by two figures to explain how the measurements were made and then summarized in Table 2. All the collar tests used the same gas-gun firing pressure and striker-bar impact speed as the test without a collar reported near the end of Section II. Ideally the stresses versus time and the stress-strain curves would have the same appearance as the curves for the no-collar specimen until the strain had reached the "predicted strain" value that just reduced the specimen length to the collar length. At this point the apparent stress-time curve would be expected to show a sharp upturn indicating the beginning of contact with the collar.

The actual results were not so ideal. Even after dispersion correction both Stress 1 and Stress 2 versus time still showed oscillations believed related to the dynamics of the loose collar, and the two stress plots did not usually reach agreement before the collar took over. Figure 15 shows Stress 1, Stress 2, Strain Rate, and Strain versus time for a specimen with predicted strain of 0.0099 for collar contact (approximately 1 percent strain or 100 on the ordinate scale). This strain is reached at

time=129 microsec, marked by a square on the strain curve. At this point both the recorded Stress 1 and Stress 2 also marked by squares, are well above the approximately 100 MPa failure stress of the no-collar test (which occurred at a strain of 0.0064 in the no-collar test). The stress records were not considered reliable for determining collar action. The strain record proved more useful.

The strain record shows a maximum strain plateau of about 0.0128 during the collar action, falling to about 0.0105 at the end of the plot, also marked by a square, after the elastic compression of the collar had been unloaded. The final value of the strain after unloading is more easily read from the stress-strain curves of Figure 16 as about 0.0102. This final unloaded value of strain is very close to the predicted strain at collar contact. The indicated stress-strain curves of Figure 16 indicate that both stresses had surpassed the no-collar test strength before this strain was reached. Both stresses show so much oscillation that it is difficult to attach significance to their apparent peaks and valleys, but it is clear that by the time the predicted strain of about 0.01 had been reached the collar was already carrying a considerable part of the load.

The strain results summarized in Table 2 show a remarkable consistency. They will be used to correlate with the crack distribution data of Section 4.2.

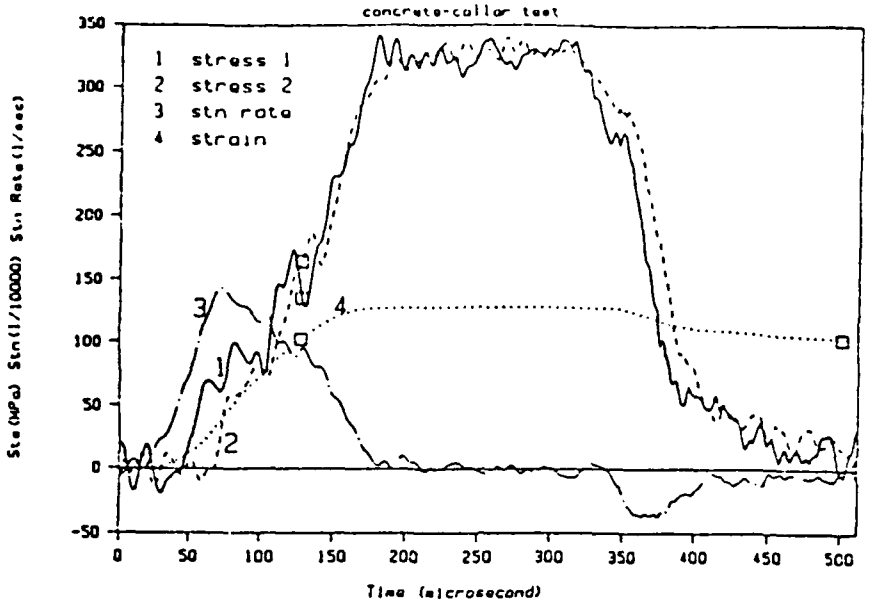

Figure 15. Stresses, strain, and strain rate versus time for collar test of Specimen No. F25.

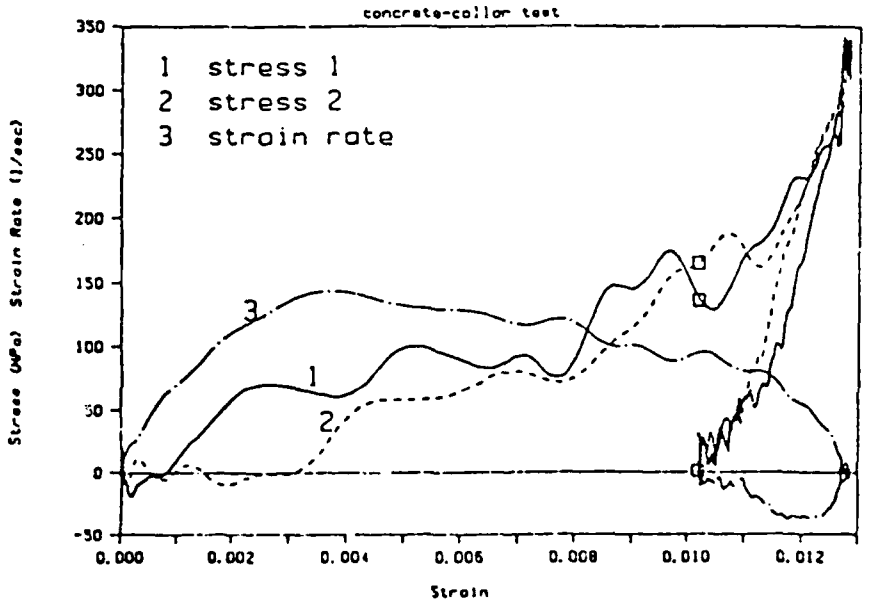

Figure 16. Stresses and strain rate versus strain for collar test of Specimen No. F25.

Table 2. PREDICTED STRAIN AT COLLAR CONTACT AND MEASURED RESIDUAL AND MAXIMUM STRAINS.

SPECIMEN No.	PREDICTED Strain	RESIDUAL Strain	MAXIMUM Strain
F21	0.0029	0.0023	0.0041
F22	0.0047	0.0046	0.0065
F23	0.0064	0.0068	0.0092
F24	0.0081	0.0082	0.0103
F25	0.0091	0.0102	0.0128
F04	0.0116	0.0106	0.0126

Figure 17 reproduces the Stress 2 versus strain curve of the no collar test of Figure 10. The six points marked on it are at the maximum strains of Table 2, indicating what points of the unconfined dynamic stress-strain curve were reached before unloading. These points represent approximately the damage conditions for the crack patterns of the dynamic collar tests to be reported in Section 4.2. Apparently the first one is at about two-thirds of the failure strain, the second one is just at the failure strain, and the other four are from the strain softening regime. This interpretation takes no account of likely random differences in the mechanical properties of the various tests specimens.

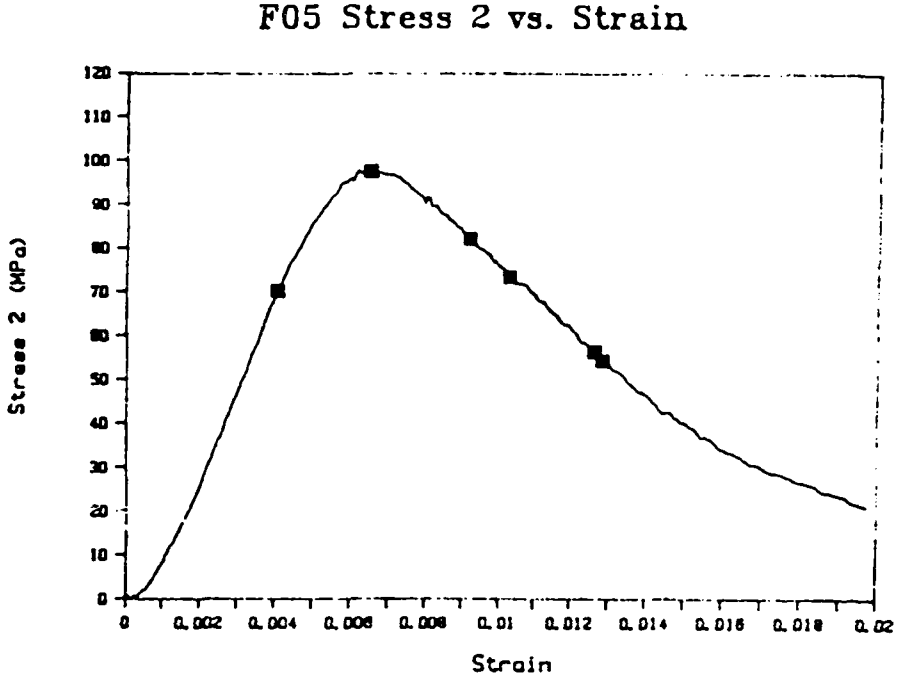

Figure 17. Dynamic stress-strain curve for no-collar test of Specimen F05 with six points marked corresponding to maximum strains in collar-interrupted tests.

Figure 18 shows a static stress-strain curve for a no-collar specimen of the same size as the dynamic test specimens (not a standard ASTM specimen). The test was performed on the 400,000-pound (1780-kN) Tinius Olsen hydraulic testing machine in the laboratory of the Civil Engineering Department of the University of Florida at a constant loading rate. The indicated strain at the peak stress is 0.010, which seems unreasonably large. The indicated strain measurements (based on head motion) include a considerable apparent strain because of slack in the system. This has been approximately corrected in the plot of Figure 19. A new zero-strain point was estimated by manually drawing a tangent back to the zero-stress level in Figure 18 from the 20 MPa point. This tangent crossed the strain axis at about 0.0042, which becomes the new zero strain point for the plot of Figure 19, with a strain of 0.0058 at the peak stress, comparable to the 0.0064 value of the dynamic tests.

No strains were actually measured in the static collar tests, carried out in a hydraulic press all to the same final load level. The maximum strains were estimated by adding to each predicted strain the strain of about 0.0002 that the elastic collar would attain if it carried all the hydraulic press load.

Three points marked on the static stress-strain curve of Figure 19 represent approximately the damage conditions for the crack patterns of three of the static collar tests to be reported

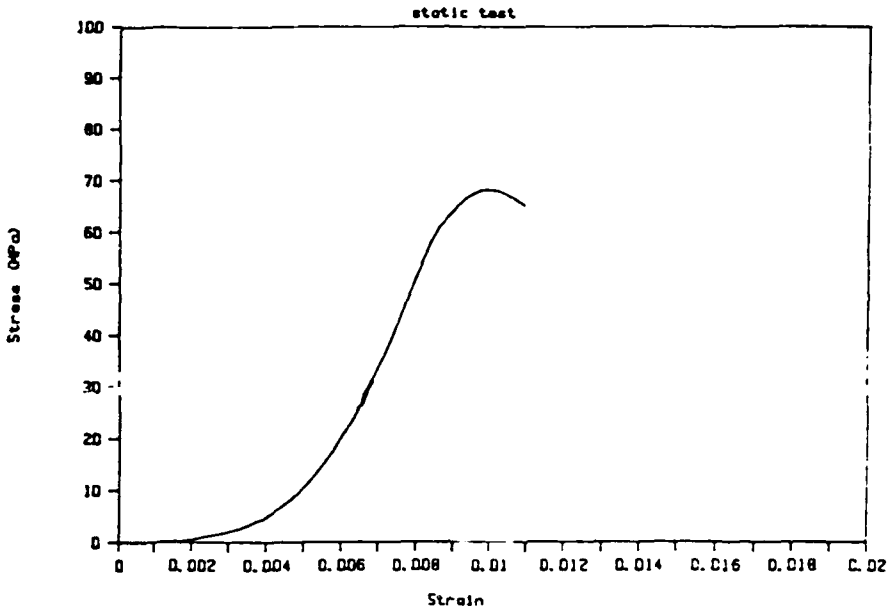

Figure 18. Recorded static stress-strain curve (no-collar Specimen F36).

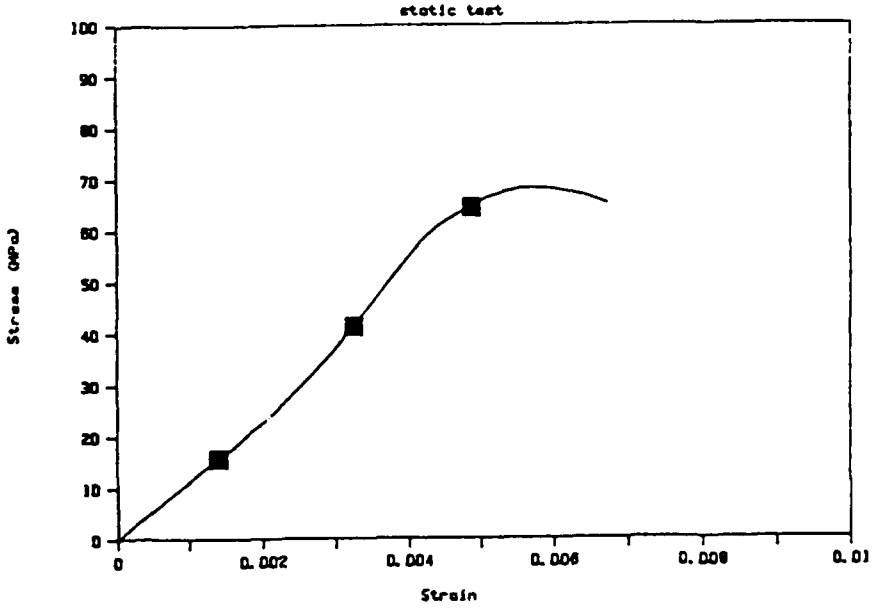

Figure 19. Static stress-strain curve of Figure 18, approximately corrected for slack in system, and marked at points corresponding to maximum strains in three collar tests.

in Section 4.2. The other three static collar-test failures occurred in the strain-softening regime, which was not recorded in the no-collar test.

4.2 Appearance of the Crack Patterns

The crack patterns for the two test series and an untested specimen are presented as Figures 20 through 32. Differences between the dynamic series and the static series are immediately apparent. In the dynamic series, the cracks are typically uniformly distributed, while the cracks in the static series specimens tend to be concentrated along definite bands between the center and the surface of the specimen. In the dynamic series, substantial cracking develops first in the specimen with predicted strain 0.0047 (measured maximum strain 0.00647) and the cracking has a similar appearance in all the longer specimens. The one shorter specimen, with predicted strain 0.0029 (measured maximum strain 0.00412), exhibited a somewhat more sparse but fairly uniform distribution of cracks. For the static series, substantial cracking first appears in the 0.0081 predicted strain specimen (no 0.0064 predicted strain specimen was sectioned) and once again the pattern of cracks is similar for the longer specimens. The three shorter specimens all exhibit a very sparse and random distribution of cracks. An untested specimen was also sectioned and examined and exhibits a small number pre-existing cracks, most of which are found within the aggregate particles.

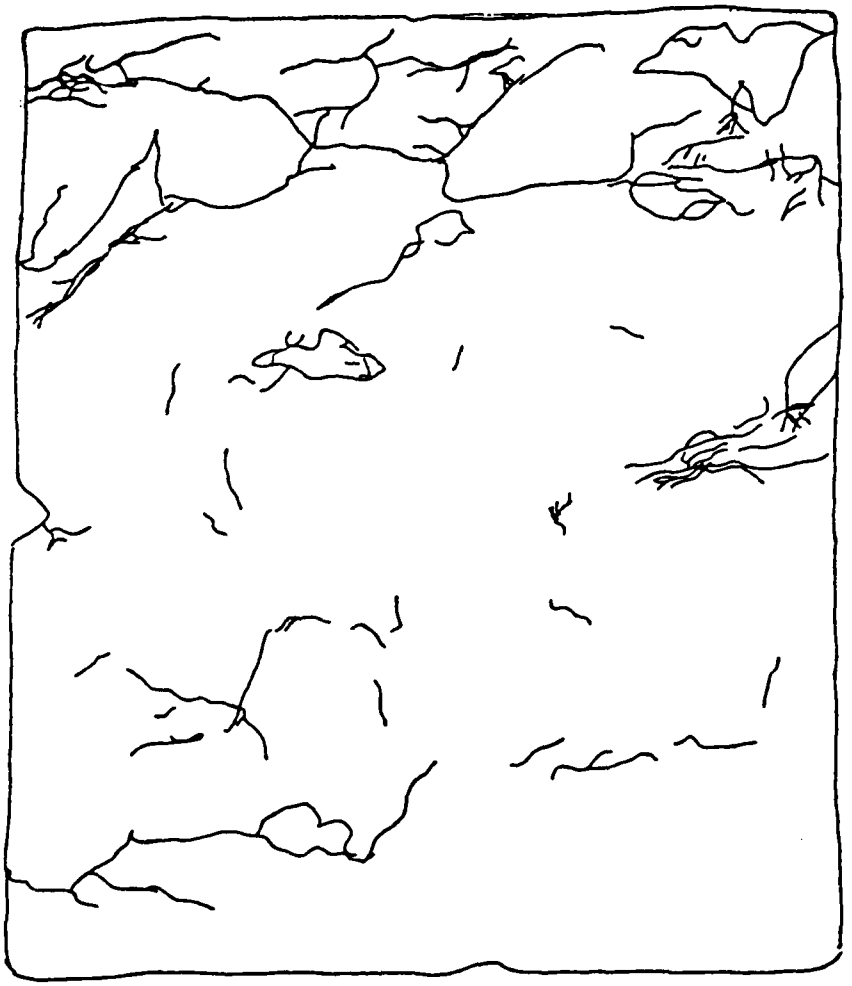

Figure 20. Crack Pattern Tracing of Dynamic Test Specimen with maximum strain 0.0041 (F21). The incident bar interface is on the left.

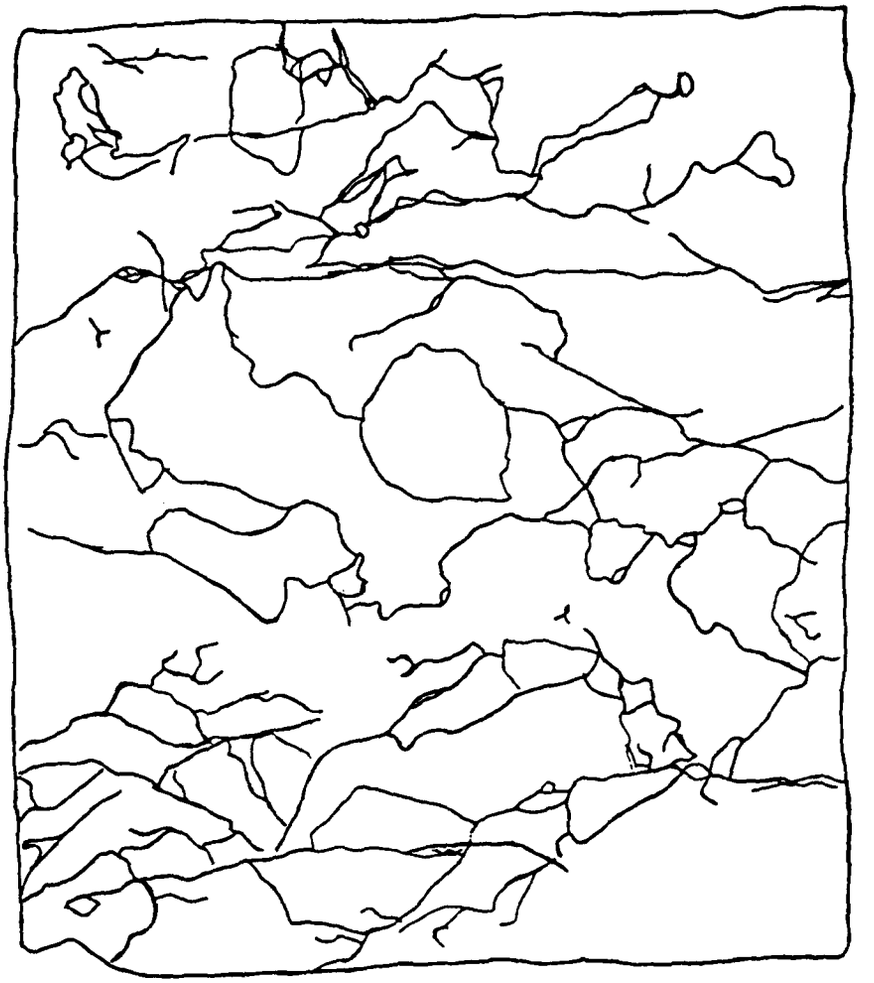

Figure 21. Crack Pattern Tracing of Dynamic Test Specimen with maximum strain 0.0065 (F22). The incident bar interface is on the left.

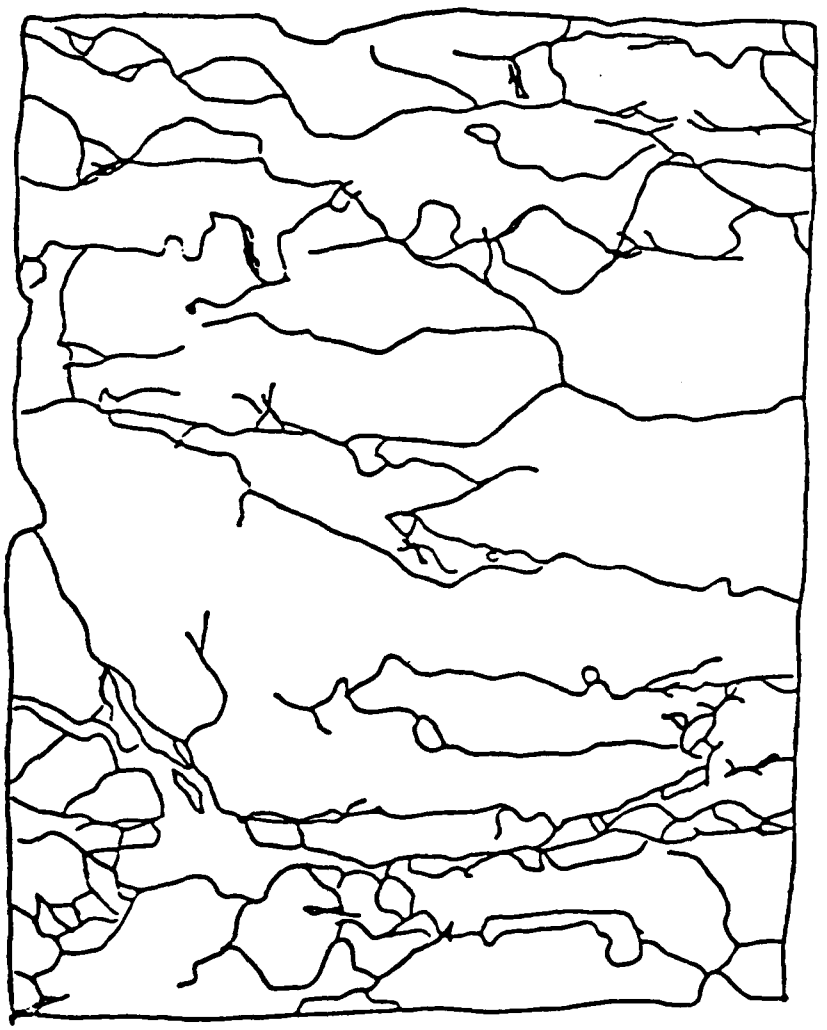

Figure 22. Crack Pattern Tracing of Dynamic Test Specimen with maximum strain 0.0092 (F23). The incident bar interface is on the left.

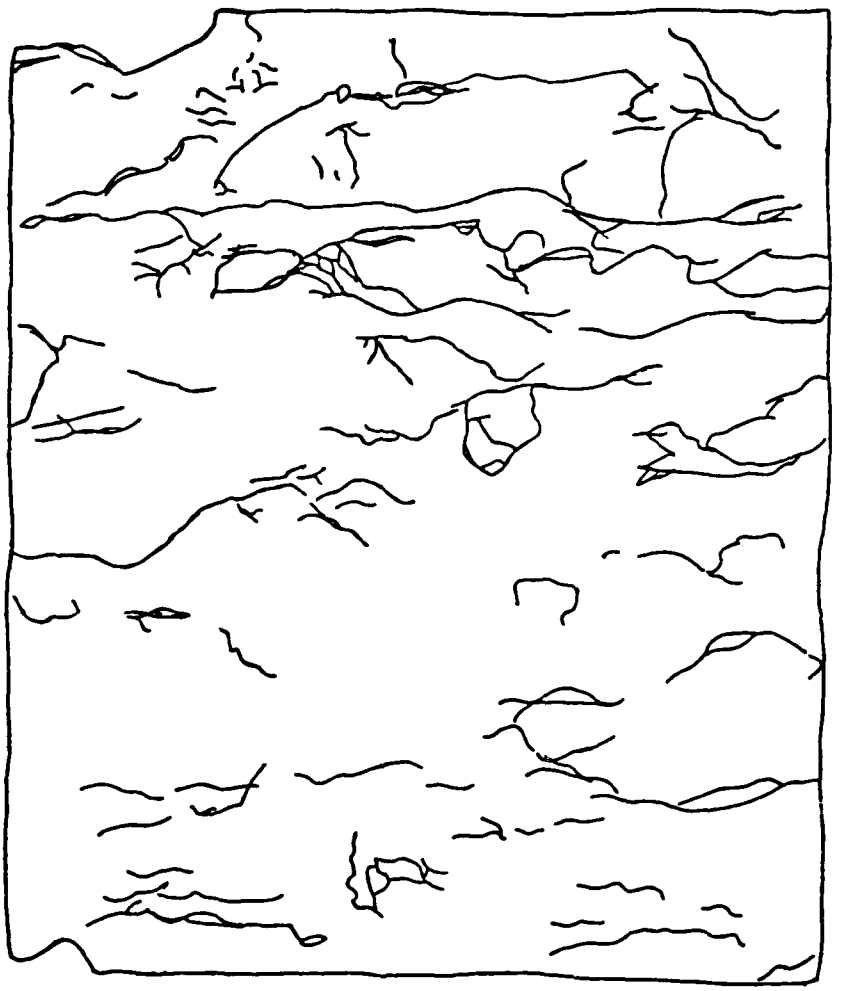

Figure 23. Crack Pattern Tracing of Dynamic Test Specimen with maximum strain 0.0103 (F24). The incident bar interface is on the left.

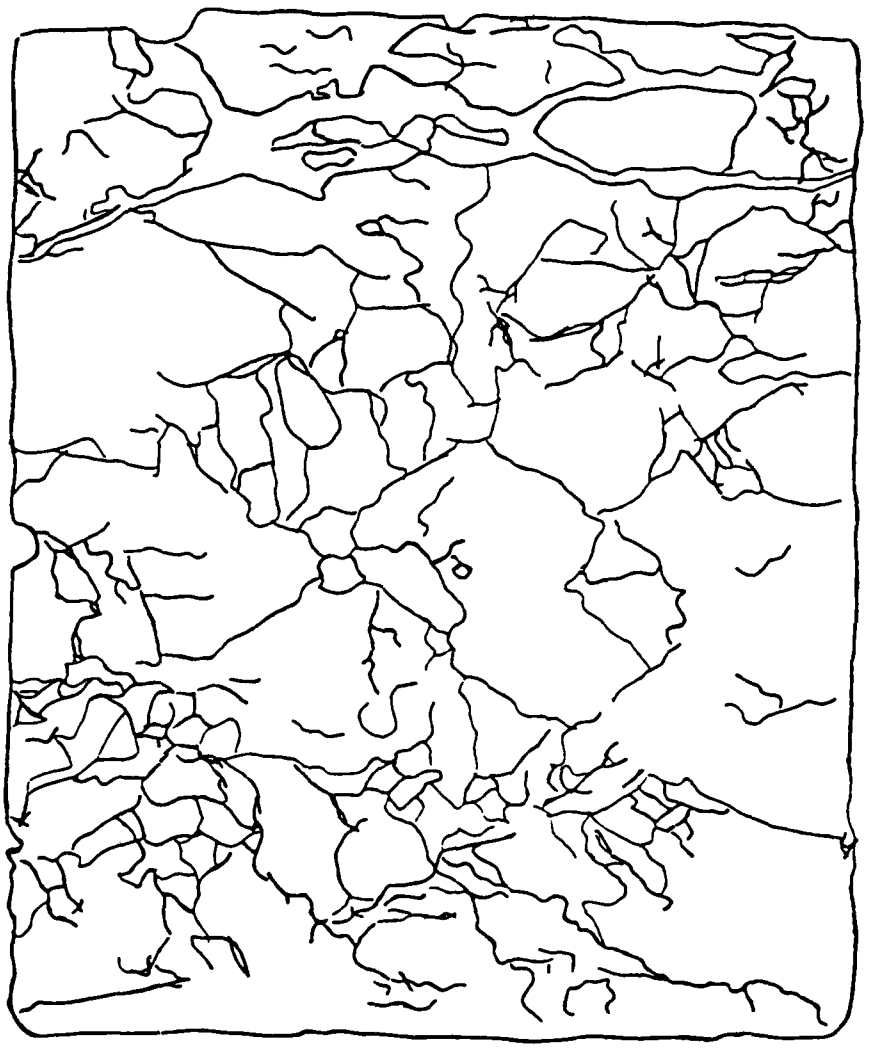

Figure 24. Crack Pattern Tracing of Dynamic Test Specimen with maximum strain 0.0128 (F25). The incident bar interface is on the left.

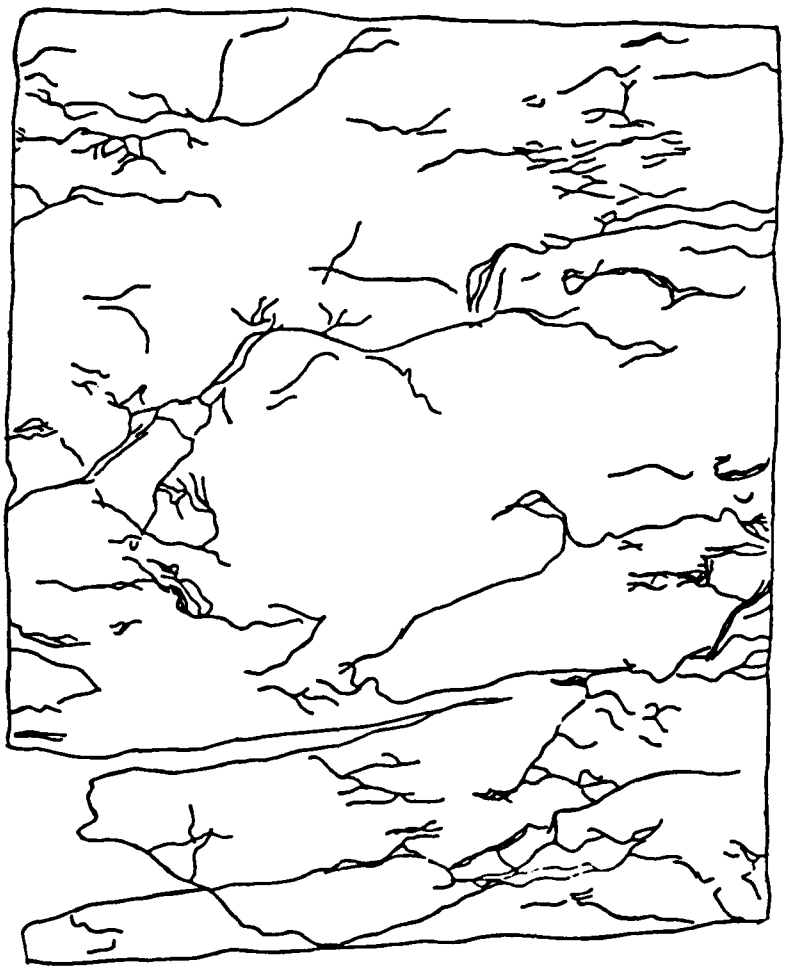

Figure 25. Crack Pattern Tracing of Dynamic Test Specimen with maximum strain 0.0126 (F04). The incident bar interface is on the left.

Figure 26. Crack Pattern Tracing of Static Test Specimen with Estimated Maximum Strain 0.0014 (F51).

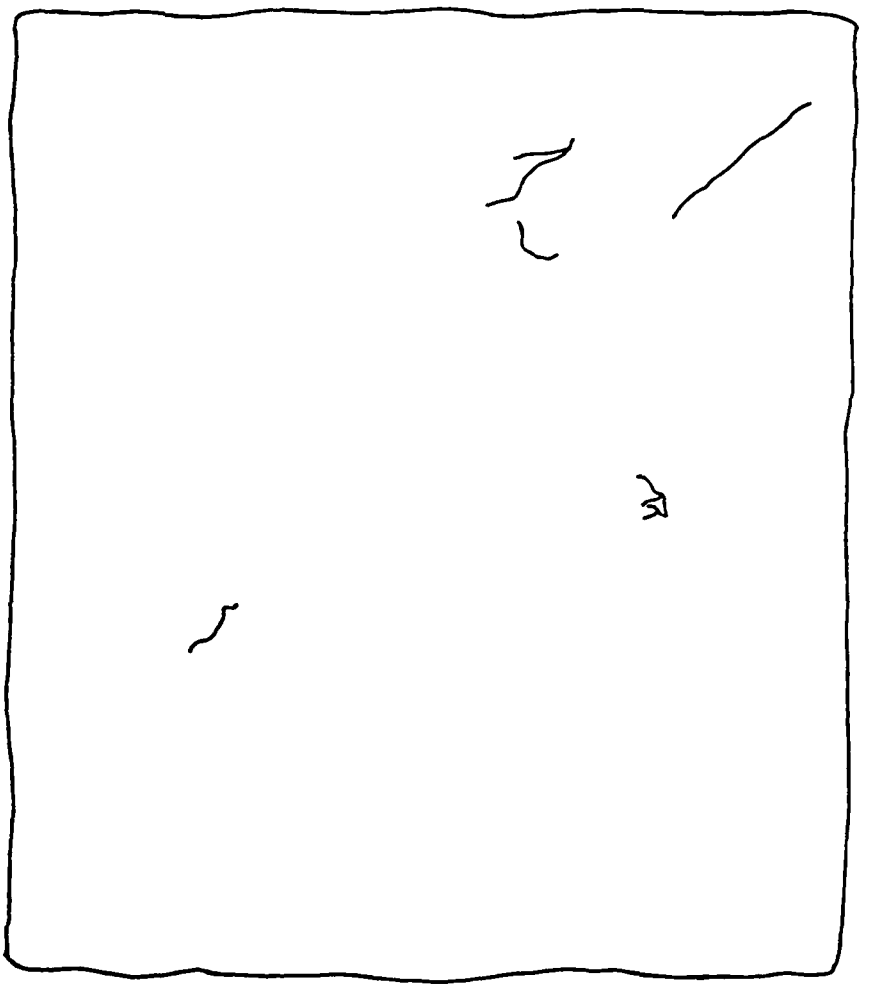

Figure 27. Crack Pattern Tracing of Static Test Specimen with Estimated Maximum Strain 0.0031 (F52).

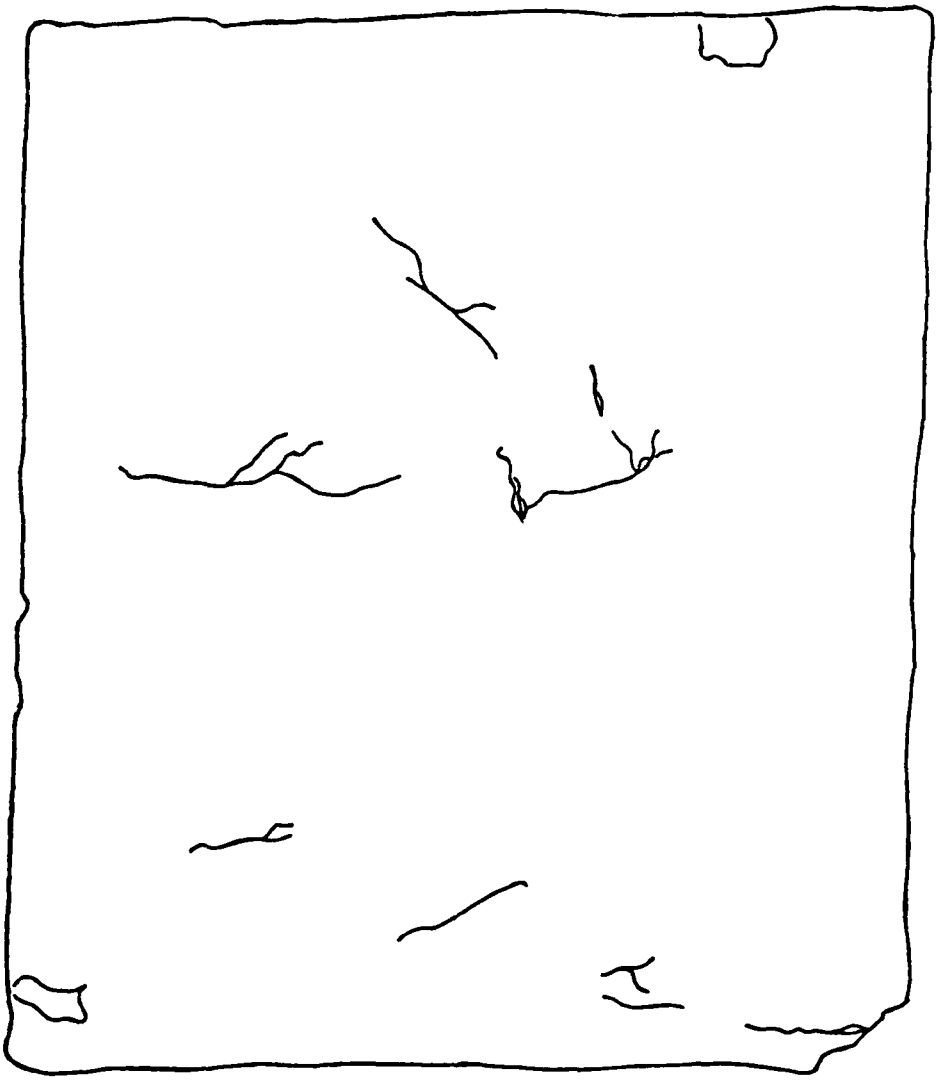

Figure 28. Crack Pattern Tracing of Static Test Specimen with Estimated Maximum Strain 0.0049 (F53).

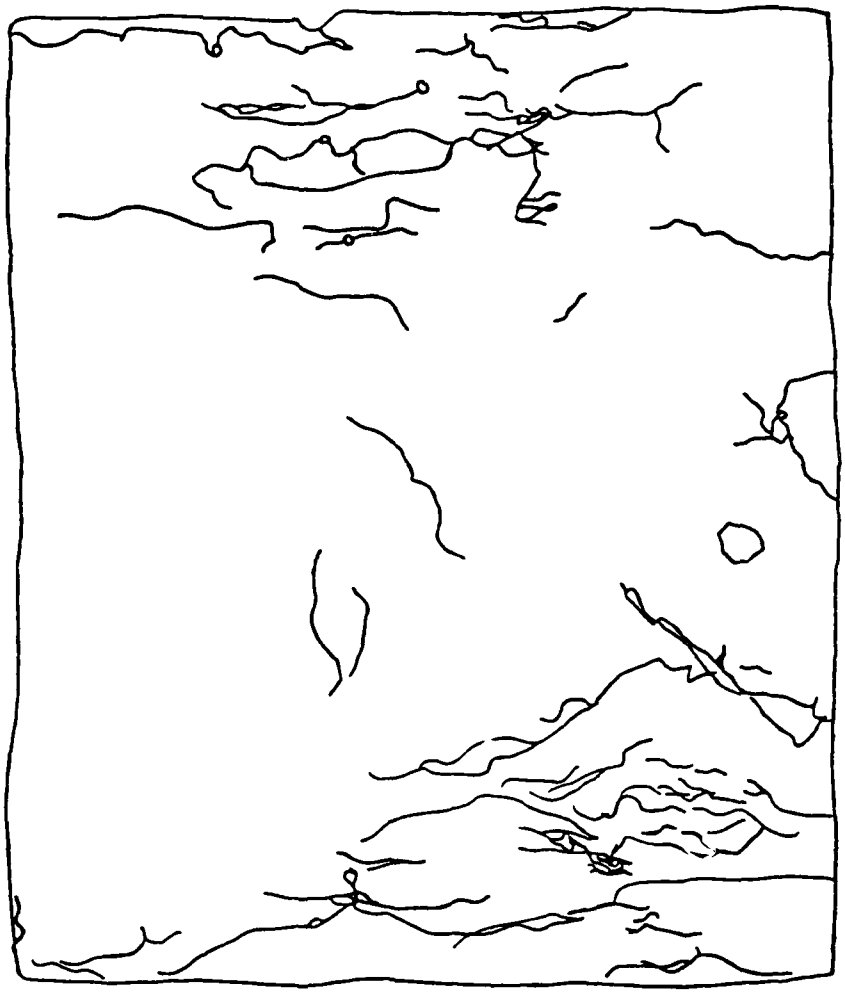

Figure 29. Crack Pattern Tracing of Static Test Specimen with Estimated Maximum Strain 0.0083 (F55).

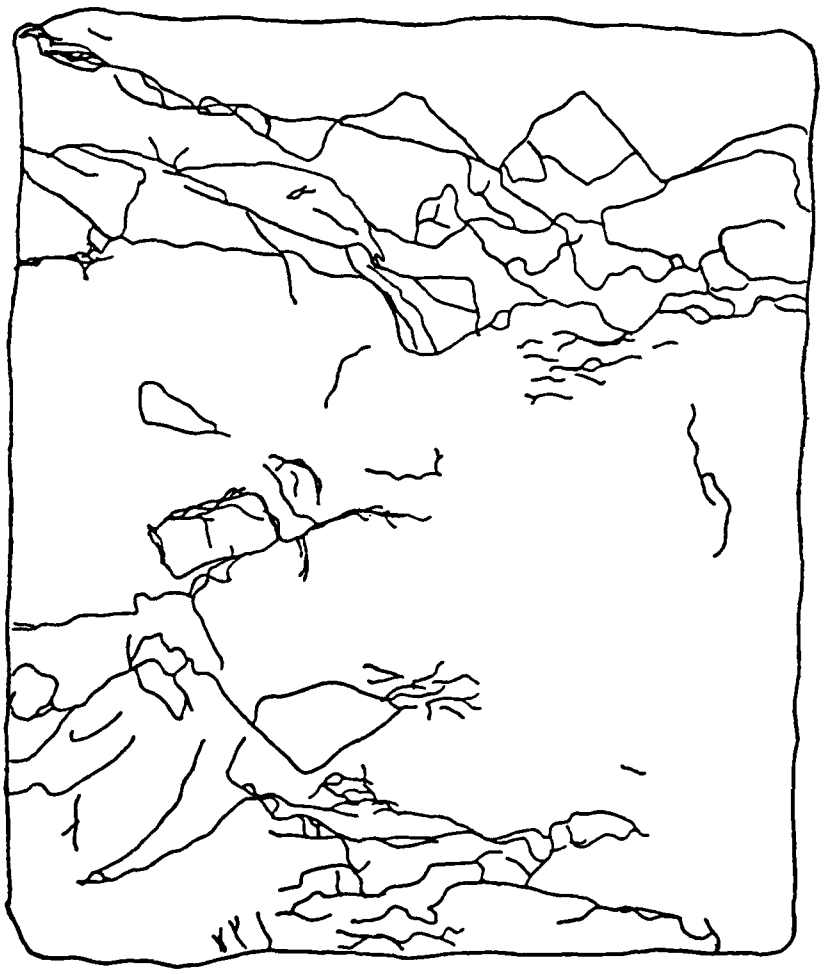

Figure 30. Crack Pattern Tracing of Static Test Specimen with Estimated Maximum Strain 0.0101 (F56).

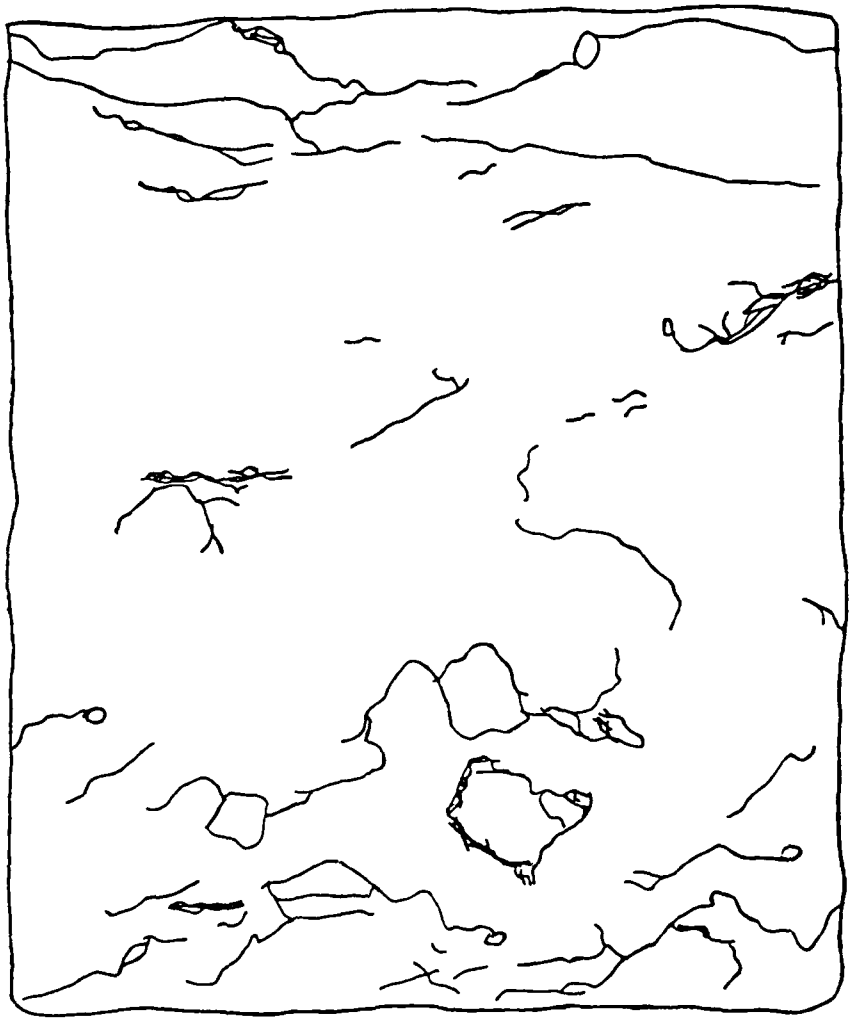

Figure 31. Crack Pattern Tracing of Static Test Specimen with Estimated Maximum Strain 0.0118 (F56).

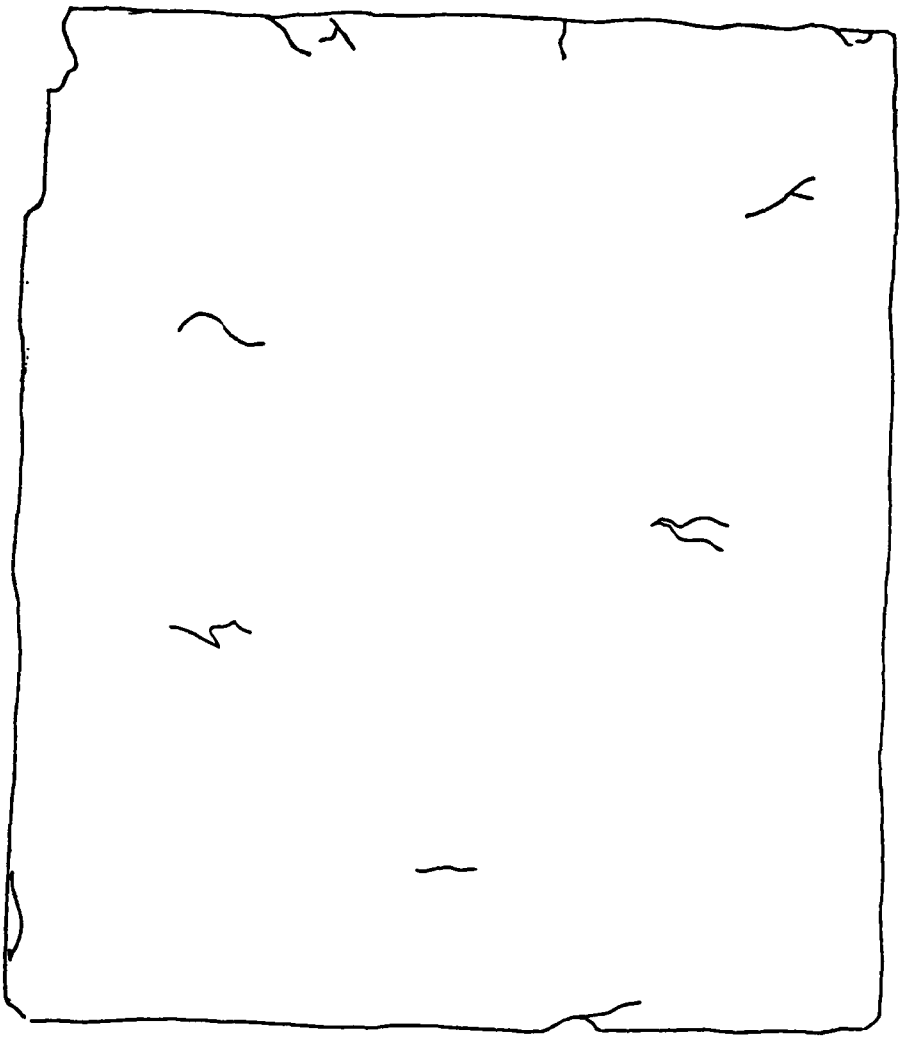

Figure 32. Crack Pattern Tracing of Untested Specimen. (F50)

4.3 Crack Surface Area

The results of the crack surface area measurements, as derived from the line intercept counting on each section, are presented in Figure 33. The surface area per unit volume is plotted against the predicted strain based on the original specimen overlength.

For maximum strains up to a threshold strain of about 0.006 (near the failure strains in no-collar tests) there is a moderate amount of cracking. Above a maximum strain of 0.006 (corresponding to the strain-softening regime in the no-collar tests) there is a significantly greater crack development. From the limited data it is not easy to confirm an upward trend of crack density with strain in either regime. For the strain-softening regime this may mean that once the major cracks have formed much of the deformation continues by sliding on the existing cracks. For the lower-strain regime, perhaps a closer examination both of the microcracks not seen by the optical microscope and of more sections from each specimen would be informative.

The very small crack density in the section from the untested specimen confirms that the the sectioning, infiltration and polishing operations do not introduce any significant cracking, so that the crack densities seen in the examination

slices may be considered to represent the condition in the test-damaged specimens before sectioning.

Figure 34 shows the same data as in Figure 34 but now plotted against the maximum strain reported in Table 2 for the dynamic tests and estimated for the static tests. It is clear that the threshold values of strain for substantial crack proliferation are much closer than those in Figure 33.

Table 3 lists the data on which Figure 33 and 34 are based: Surface Area per Unit Volume, Predicted Strain and Maximum Strain for each specimen.

The line intercept counts were repeated and intercepts totaled separately for cracks entirely in the mortar, cracks entirely in the aggregate particles and cracks at the interface between the aggregate and the mortar. The results of these measurements are shown in Table 4. No dramatic differences are apparent between the three categories, but it is clear that for this particular concrete, which has relatively soft and weak aggregate, the aggregate and the aggregate/mortar interface provide a large share of the total crack area in each specimen.

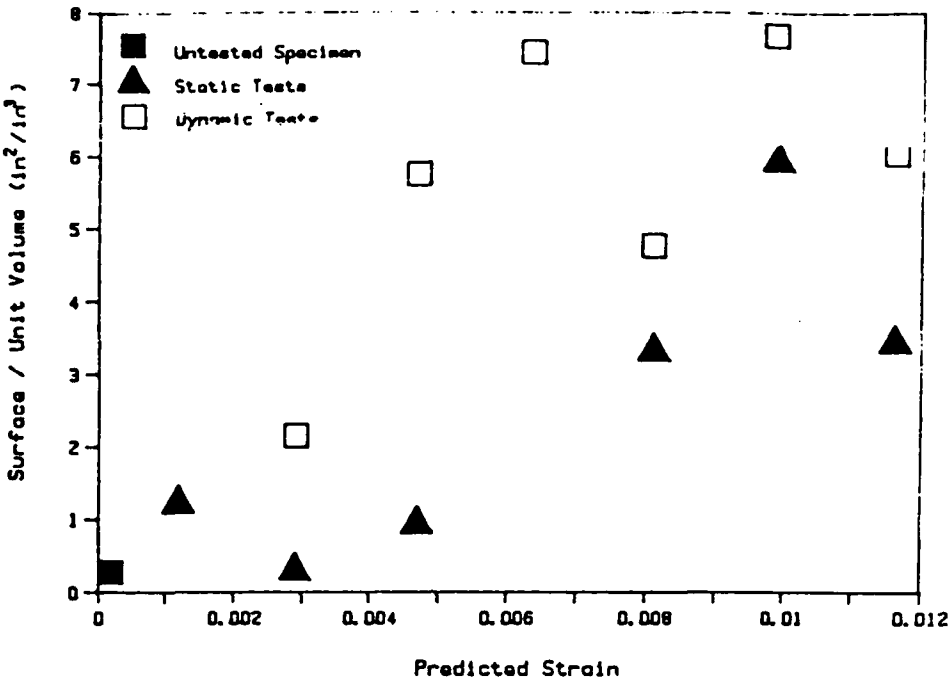

Figure 33. Crack surface per unit volume versus predicted strain.

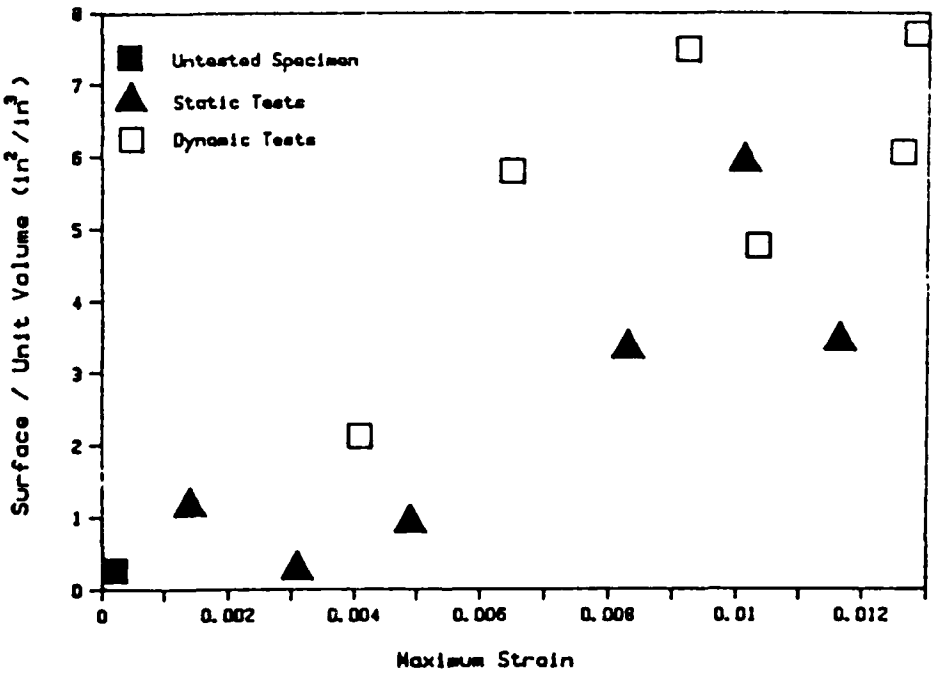

Figure 34. Crack surface per unit volume versus maximum strain.

Table 3. Crack Surface Area per unit volume at various strain levels.

Dynamic Test Results

Specimen No.	Predicted Strain	Maximum Strain	Surface/Unit Volume
F21	0.0029	.0041	2.14
F22	0.0047	.0065	5.78
F23	0.0064	.0092	7.46
F24	0.0081	.0103	4.76
F25	0.0099	.0128	7.68
F04	0.0116	.0126	6.06

Static Test Results

Specimen No.	Predicted Strain	Estimated Maximum Strain	Surface/Unit Vol. (in^2/in^3)
F51	.0012	.0014	1.16
F52	.0029	.0031	0.28
F53	.0047	.0049	0.94
F54	.0081	.0083	3.34
F55	.0099	.0101	5.92
F56	.0116	.0118	3.46

Untested Specimen

F50			0.2

Table 4. Raw Intercept Counts (crack location discriminated)

Predicted Strain	Interface	Aggregate	Mortar
	Static Tests		
0.0012	108	42	10
0.0029	14	23	1
0.0047	57	22	22
0.0081	155	91	210
0.0099	199	184	383
0.0116	186	121	174
	Dynamic Tests		
0.0029	89	90	105
0.0047	318	163	308
0.0064	298	214	353
0.0081	222	167	258
0.0099	276	152	702
0.0116	177	242	294
	Untested		
-	5	30	10

SECTION V

CONCLUSIONS AND RECOMMENDATIONS

The following conclusions are supported by the experimental investigation reported in Sections III and IV, in which both static and dynamic tests on specimens of one particular concrete were interrupted by a steel collar shorter than the specimens, so that intact damaged specimens could be examined for macrocrack development.

CONCLUSIONS

1. A substantial increase in crack surface area per unit volume occurs at a threshold strain near the strain at peak stress in the no-collar tests.
2. The threshold strains of the dynamic and static tests are about the same.
3. Despite considerable scatter and limited data, it appears that the crack surface per unit volume is considerably higher in the dynamic tests than in the static tests at the same level of maximum strain. This presumably means that in the static tests there tends to be on the average more sliding on each crack than in the dynamic tests.

4. The distribution of cracks is fairly uniform in the dynamic-test specimens, while there is a tendency for dense bands of cracks to form in the static tests.
5. The aggregate and the aggregate/mortar interface provide a considerable portion of the total crack area in this particular concrete. No great difference between the static and dynamic tests was noted in this respect.
6. The collar method was successful in arresting the tests, so that intact damaged specimens were recovered for examination, and it was possible to deduce the maximum strain level reached in the tests.
7. The sectioning, infiltration, and polishing did not introduce any significant macrocracking in the specimens. Thus, the macrocrack patterns observed are representative of the damage conditions at the end of the tests.

RECOMMENDATIONS

1. The results of this very limited investigation are so promising that a more extensive investigation along these lines seems warranted. The following specific recommendations should be considered in any extended investigation.
2. Specimens near the threshold strain are especially interesting. A closely spaced series to precisely map out the threshold region would be useful, and it should be

possible to take a closer look at the process zones around the developing cracks, possibly using Scanning Electron Microscope methods.

3. More sections, on some specimens at least, should be taken to improve the statistics and reduce any orientation bias.
4. Stress measurements in the dynamic tests might be improved by more accurate alignment of the collar and use of strain gages on the elastic collar, which should make it possible to determine the load carried by the collar, so that the load carried by the concrete could be calculated.
5. The furfural alcohol infiltration method was successful in revealing the macrocracks, but the crack identification was a tedious process because of the prominence of other micrographic features. It should be possible to facilitate the procedure by adding a fluorescent dye to the furfural alcohol before infiltration into the cracks and using ultraviolet illumination, so that only the cracks will show up in the micrograph. It might then be possible to automate the crack counting. Fluorescent-dye techniques have been reported previously in examination of very thin slices to observe porosity and microcracking; see References 8 to 10. they should also be useful to observe the macrocracks in thicker slices.

SECTION VI

REFERENCES

1. L. E. Malvern, T. Tang, D. A. Jenkins and J. C. Gong, "Dynamic Compressive Strength of Cementitious Materials,", Materials Research Society, Symposium Proceedings, Vol. 64, 119-138, 1986.

2. Malvern, L. E. and C. A. Ross, Dynamic Response of Concrete and Concrete Structures, Final Technical Report, Contract AFOSR F49620-83-K007, University of Florida, 30 May 1986.

3. L. E. Malvern, D. A. Jenkins, T. Tang and C. A. Ross, "Dynamic Compressive Testing of Concrete," Proc. Second Symposium on the Interaction of Non-Nuclear Munitions with Structures, Panama City Beach, Florida, April 15-19, 1985, pp. 194-199.

4. T. Tang, L. E. Mallvern and D. A. Jenkins, "Dynamic Compressive Testing of Concrete and Mortar," Engineering Mechanics in Civil Engineering, eds. Boresi, A. P. and Chong, K. P., ASCE, New York, 1984, 663-666.

5. P. S. Follansbee and C. Frantz, "Wave Propagation in the Split Hopkinson Pressure Bar," ASME Journal of Engineering Materials and Technology, Vol. 105, 61-66, 1983.

6. C. W. Felice, The Response of Soil to Impulse Loads Using the Split-Hopkinson's Pressure Bar Technique, Ph. D. Dissertation, The University of Utah, 1985.

7. E. E. Underwood, "Surface Area and Length in Volume," pp. 78-125 in Quantitative Microscopy, eds. R. T. DeHoff and F. N. Rhines, McGraw Hill, New York 1968.

8. K. L. Gardner, "Impregnation technique using colored epoxy to define porosity in petrographic thin sections," Canadian Journal of Earth Sciences, Vol. 17, pp. 1104-1107, 1980.

9. L. E. Knab, H. N. Walker, J. R. Clifton and E. R. Fuller, Jr., "Fluorescent Thin Sections to Observe the Fracture Zone in Mortar," Cement and Concrete Research, Vol. 14, pp. 339-344, 1984.

10. L. I. Knab, H. Jennings, H. N. Walker, J. R. Clifton and J. W. Grimes, "Techniques to Observe the Fracture Zone in Mortar and Concrete," pp. 241-247 in Fracture Toughness and Fracture Energy of Concrete, ed. F. H. Wittmann, Elsevier Science Publishers, Amsterdam, 1986.

APPENDIX

Figures A-1 through A-13 are macrophotographs of infiltrated and polished sections of each specimen (about 1.7X)

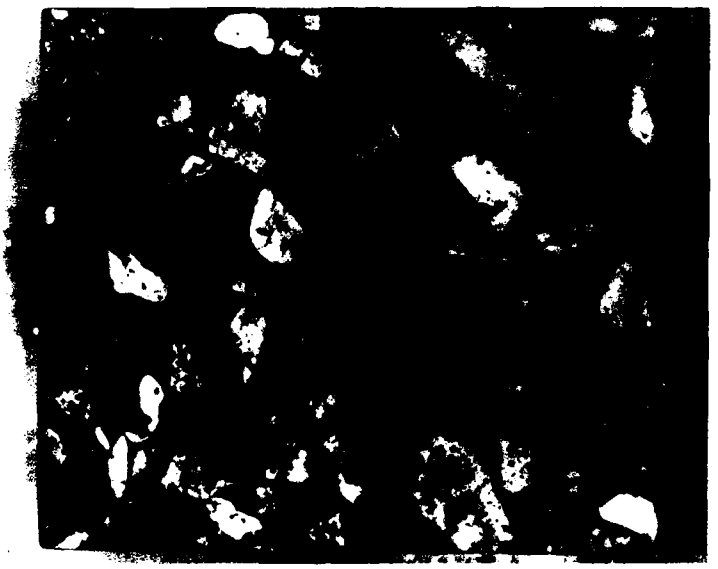

Figure A-1 Dynamic Test Specimen F21

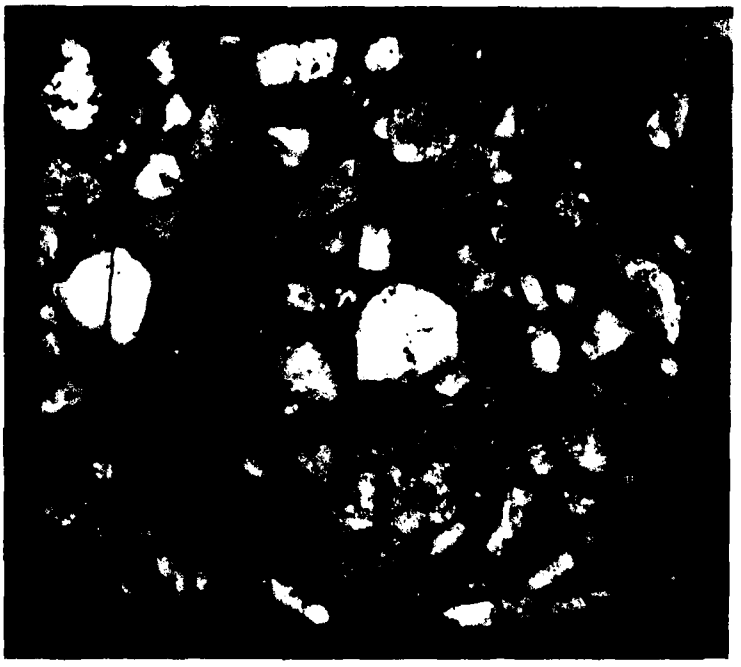

Figure A-2 Dynamic Test Specimen F22

Figure A-3 Dynamic Test Specimen F23

Figure A-4 Dynamic Test Specimen F24

Figure A-5 Dynamic Test Specimen F25

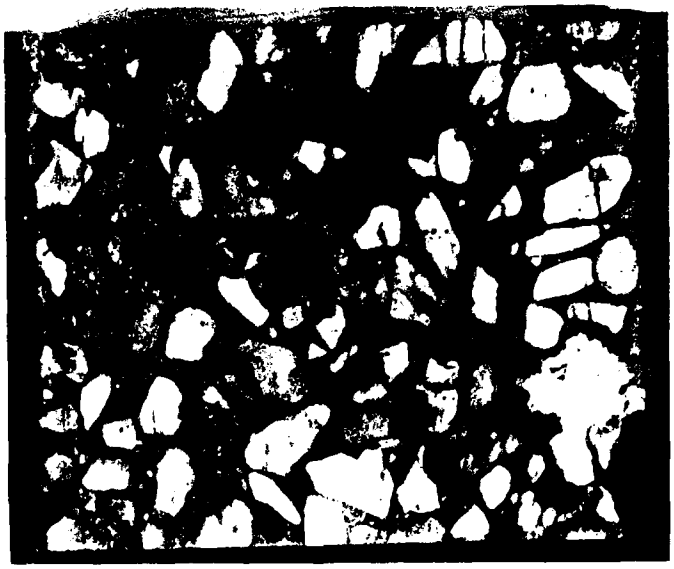

Figure A-4 Dynamic Test Specimen F24

Figure A-5 Dynamic Test Specimen F25

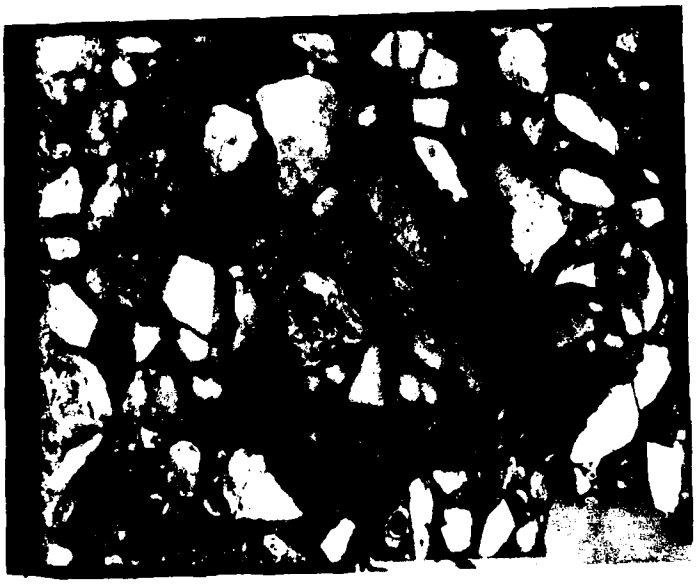

Figure A-6 Dynamic Test Specimen F04

Figure A-7 Static Test Specimen F51

Figure A-8 Static Test Specimen F52

Figure A-9 Static Test Specimen F53

Figure A-10 Static Test Specimen F54

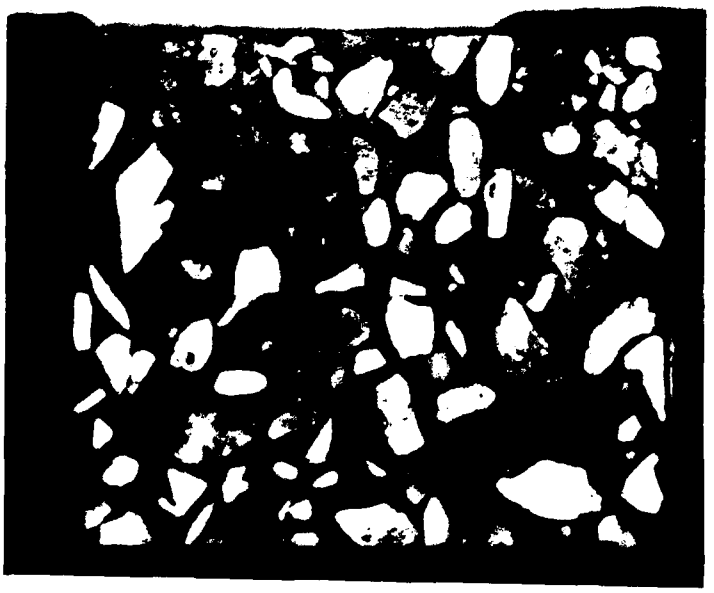

Figure A-11 Static Test Specimen F55

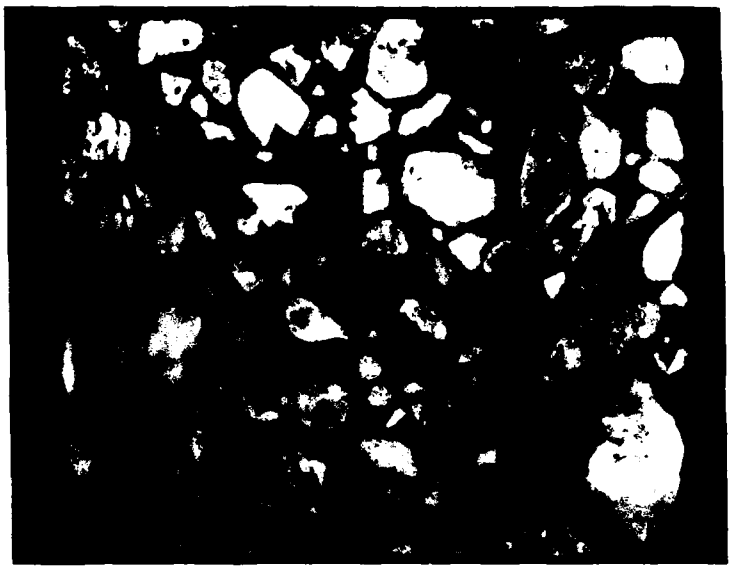

Figure A-12 Static Test Specimen F56

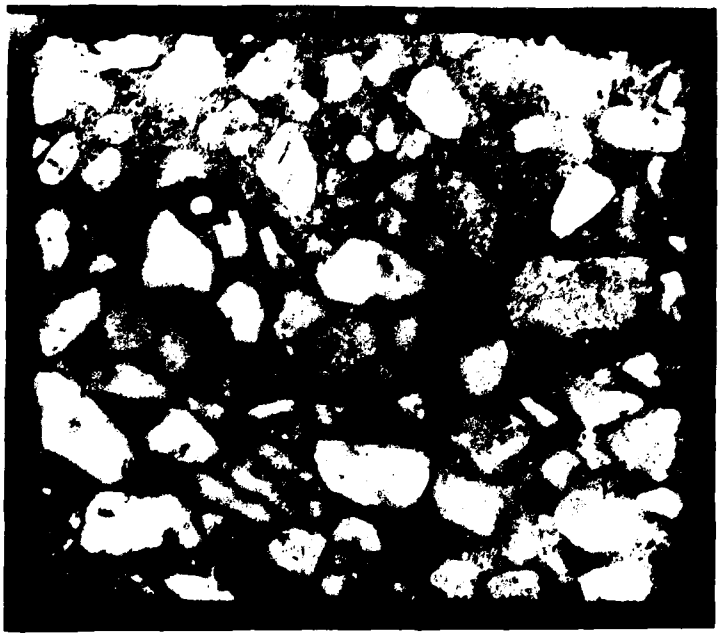

Figure A-13 Untested Specimen F50